The Dissertation Committee for Franklin Bhogaraju Grigsby
certifies that this is the approved version of the following dissertation:

Chirped Pulse Raman Amplifier

Committee:

Michael W. Downer, Supervisor

Lothar W. Frommhold

Michael F. Becker

John W. Keto

Greg O. Sitz

Chirped Pulse Raman Amplifier

by

Franklin Bhogaraju Grigsby, B.S.

Dissertation

Presented to the Faculty of the Graduate School of

The University of Texas at Austin

in Partial Fulfillment

of the Requirements

for the Degree of

Doctor of Philosophy

The University of Texas at Austin

December 2009

This thesis is dedicated to my parents.

Acknowledgments

I would like to thank many people. First of all, I would like to thank my research supervisor Dr. Michael Downer, who has supported me through my graduate career and has shown me how to conduct research. As I grew and as I struggled in the world of physics, he was there to give me suggestions and taught me patience. It is with his help that I have grown as a researcher. I would like to thank all the members of my research group who have worked with me over the years, Rafal Zdadzag, Bonggu Shim, Nicholas Matlis, Ben Bowes, Peng Dong, and P.J. Smith. Finally, would like to thank my parents without whom I wouldn't be here in this world and without whose support I wouldn't have been able to finish this work.

Franklin Bhogaraju Grigsby

The University of Texas at Austin

December 2009

Chirped Pulse Raman Amplifier

Publication No. _____

Franklin Bhogaraju Grigsby, Ph.D.
The University of Texas at Austin, 2009

Supervisor: Michael W. Downer

All modern terawatt- and petawatt-class laser systems are based on the principle of chirped-pulse amplification (CPA). In this work, a compact subsystem that shifts a micro-joule portion of the chirped pulse energy to a new wavelength outside its original bandwidth, then amplifies it to millijoule energy without adding pump lasers, and without compromising the output of the fundamental CPA system in any significant way, has been developed and integrated into a standard terawatt-class CPA system. In this chirped pulse Raman amplifier sub-system, a 30 mJ portion of a chirped 800 nm fundamental pulse within the CPA system was split into two unequal portions, each of which impinged on a Raman-active barium nitrate, or Ba(NO3)2, crystal of length 5 cm. The weaker portion created a weak (15 J) first Stokes pulse (873 nm) by Stimulated Raman Scattering (SRS) in the first crystal, which then seeded a non-collinear four-wave-mixing process driven by the stronger portion of the split-off CPA pulse in the second crystal. The latter process amplified the first Stokes seed pulse to several millijoules with excellent beam quality. A study of Raman gain as a function of time delay between pump and Stokes pulse in the second crystal revealed a sharply peaked narrow interval ($\sim$ 3 ps FWHM) of

high gain and a wider interval ($\sim$ 50 ps) of low gain. The amplified, chirped first Stokes pulse was successfully compressed to 100 fs duration using a grating pair of different line density than in the main CPA system, based on a comprehensive dispersion analysis of the optical path of the first Stokes pulse. The possibility of generating higher-order Stokes and anti-Stokes sidebands of the CPA pulse is also demonstrated. Further amplification of the sideband pulse by conventional methods, using an additional pump laser, appears straightforward. The chirped pulse Raman amplifier provides temporally synchronized fundamental and Raman sideband pulses for performing two-color, high-intensity laser experiments, some of which are briefly discussed. It can be integrated into any standard CPA system, and provides significant new versatility for high-intensity laser sources.

Contents

Chapter 1

Motivations for High Intensity Two Color Experiments

1.1 Introduction

In this chapter, high field experiments using a two color laser previously not constructed are outlined. New physics including coherent control of high intensity processes is given. Advances on previous state of the art experiments as well as practical advantages of a two color high intensity laser source are given.

In many high-field experiments it is desirable to accompany the main terawatt (TW) pulse with a moderately powerful (~ 0.1 TW), temporally synchronized ultrashort pulse at a slightly shifted ($\Delta\lambda \leq 100$ nm) center wavelength outside the bandwidth of the main pulse. Such a secondary pulse can serve *e.g.* as a spectrally distinct, low group-velocity-walkoff probe in cm-scale plasma waveguides,[2] or to induce beat-frequency modulation on the main pulse in order to seed the growth of a plasma wakefield[1] via the forward Raman instability [3]. Three-wave parametric processes in nonlinear crystals cannot produce such small $\Delta\lambda$ because of IR absorption of the idler wave. To avoid this problem, Zhavoronkov *et al.*[4] demonstrated

the generation of 80 μJ, sub-GW, 870 nm pulses by stimulated Raman scattering (SRS) of chirped 1.5 mJ, 800 nm pulses in barium nitrate, followed by recompression to $\sim$ 190 fs. Because it uses chirped pulses to avoid damage and self-phase modulation in the Raman-active medium, this technique is well suited to TW-scale laser systems based on chirped pulse amplification (CPA), but previously has been demonstrated only on a much lower power system[6].

Most experiments in the field today are done at one wavelength. It is generally desirable to have two colors, synchronized, close together in wavelength that are arbitrarily amplifiable. The Chirped Pulse Raman Amplifier (CPRA) detailed below accomplishes this. Peak intensities of state of the art, high power, lasers at focus yield energy densities greater than what could be achieved if the power of the sun incident on the whole face of the Earth (10^{17} W) was focused to one square centimeter. The electric fields generated by high intensity optical lasers will move free electrons in this light to velocities approaching the speed of light in vacuum. Given a laser with a peak intensity characterized by the parameter a_o, the normalized vector potential, which is given here relative to the velocity v with which a free electron moves in its electric field as $a_o = \frac{v}{c}\frac{1}{1-v^2/c^2}$ in the weakly relativistic limit. The normalized vector potential is approximately the ratio of the speed of an electron to the speed of light at low velocities, so it is a good measure of a laser for high field work in plasmas. For $a_o \sim 1$, velocities near the speed of light, the force created by gradients in the intensity of the laser push electrons away from ions into density depressions and peaks that are of the same magnitude as the ambient plasma density. The field left behind after the laser is gone, due the plasma displacement, is known as the wakefield. The ponderomotive force from the laser creates fields parallel to the laser as it propagates with the same strength as hold together atoms. By taking advantage of the accelerating field created through large displacement of plasma, it is a possibility to get TeV electrons in a few meters of propagation.

To actually realize laser plasma based particle acceleration, a host of instabilities that exist at the large fields, velocities, and energy densities must be dealt with [3]. A key result that motivated the work presented here on the production of a high power two-color laser source is the work of Fomyt'skyi et al. on Raman seeding the laser wakefield [3]. That works shows that introducing a second laser separated in frequency by the plasma frequency stabilizes the acceleration process, lowers the intensity threshold needed for large plasma displacements, and yields a large amount of relativistic charge.

1.2 Raman Seeded Self-Modulated Laser Wakefield Accelerator

Laser-plasma interactions are interesting because it is rare to find the high concentration of energy as is common when a high power laser is focused in a plasma. A solid or liquid material that is present at the focus of such as laser will have its bound electrons ripped off of it. This process of ionization is commonly seen as laser damage. In fact, a normally transparent gas, such as nitrogen, helium, or another noble gas will also be split apart into its positively and negatively charged constituents. The plasma thus created is the only substance not damaged when it interacts with the laser. It can not be damaged because it is already broken down. The breakdown of gasses is a convenient method of generating homogeneous high density plasmas.

The Raman-seeded Self-Modulated Laser Wakefield Accelerator is exciting as a source of relativistic particles with low emittance. It has the possibility to be highly efficient at transferring energy from the wall current to relativistic electrons and can operate at low energies. The possibility of acceleration at sub-critical powers for relativistic self-focusing exists. Also, channelled RS SM-LWFA affords the possibility

of high energies in a particle beam from a tabletop laser system.

The Raman seeded SM-LWFA was first proposed by Tajima[1]. A self-modulated laser wakefield is plasma wave produced by a powerful laser pulse acting as a driver of the wave. The plasma wave is strong enough that background electrons will become trapped in the accelerating portion of the wave. Nano-coulombs of charge moving at relativistic speeds can be produced. However, the self-modultated wakefield is not as efficient or as controlled as RS-LWFA. The RS SM-LWFA allows controlled plasma wave generation and particle acceleration. By seeding the forward Raman scattering instability, trapping and subsequent acceleration of background plasma electrons is possible by low energy pulses (even less than 0.1 J) that copropagate with 1 percent energy seed pulses shifted in wavelength [3]. 1D and 2d PIC simulations by Fomyts'kyi show that as low as 38 mJ at 800 nm can yield 0.5 nC of relativistic charge.

Fomyts'kyi showed that a driving pulse of frequency ω seeded with a co-propagating pulse with a much lower intenstiy and a frequency $\omega_{seed} = \omega - \omega_p$ generates a resonance modulation which splits the pulses up into energy packets of length the plasma period. The resonant energy packets resonantly drive a plasma wave which generates a high amplitude plasma wave. In contrast to the traditional plasma beatwave experiment, the two pulses are not of comparable intensity and the density is typically orders of magnitude higher. The idea is to injection seed the SM-LWFA similar to what is done in Raman amplifiers as will be described later. Spontaneous pickup of background electrons into the acceleration regime of the plasma wave generates a beam of relativistic electrons. The RS SM-LWFA has been shown to operate as a high efficiency, low energy injector [3].

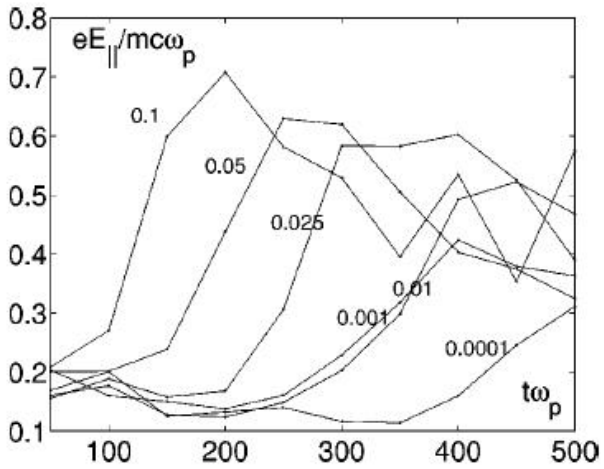

Figure 1.1: Wakefield amplitude for different values of seed amplitude as a function of interaction time. [3]

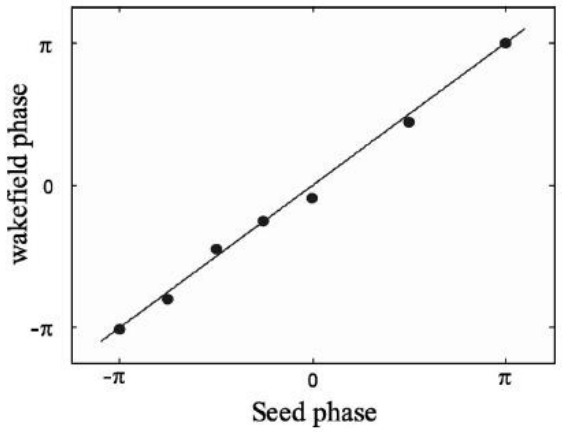

Figure 1.2: Wakefield phase vs seed phase $a_o = 0.5$, t = 200 ω_p^{-1}, ten percent seed. Raman seeding allows control of the phase of wave which is excited. [3]

The two figures from the cited work of Fomyts'kyi show that the seed enhances the LWFA greatly. It provides an increase in the growth rate even for a very low seed amplitude. This makes sense as the background level from which the SM-LWFA grows is very low. Even more excitingly, the phase of the plasma wave can be coherently controlled. The phase of the wave is the phase of the seed. This is clearly shown in the figure. The dephasing length of the wakefield is the distance over which an electron will outrun the accelerating part of a wave and no longer gain further energy. The RS SM-LWFA overcomes this by allowing for multiple stages where the phase is controlled in each stage to rephase the electron with the accelerating part of the wave. Overall, the RS SM-LWFA is exciting because it allows the injection and acceleration of electrons at low energy and power, it increases efficiency in the transfer of energy from wall current to those electrons, and it allows coherent control of the plasma wave generated. This theoretical result motivated the work presented here for the creation of an optical source that could seed the laser wakefield.

1.3 The Beatnote Electromagnetic Cascade

Another promising new scheme is Laser Pulse Compression Using Electromagnetic Cascading in Plasma by Kalmykov and Shvets [5]. This is different than forward Raman scattering as the laser driver creates a periodic index of refraction in the plasma in time which coherently scatters the wave into sidebands, beatnotes. The Group Velocity Dispersion (GVD) in plasma can cause compression of this broadened bandwidth leading to an increase in peak intensity. The Barium Nitrate CPA Raman shifter described here can be used in such a scheme and it can yield pulses that are a few cycles long. This high energy, high intensity compression scheme has applications for current and future high energy lasers which are so intense that they would damage any solid compressor.

The beatnote scheme goes against the premise of chirped-pulse amplification which is the standard for high power ultrafast pulses. A CPA system spreads the pulse out in time to prevent nonlinearities from negatively impacting the pulse as it is amplified to high energy. A separate compressor is then used to bring all the colors into phase and yield a high power source. The beatnote scheme uses plasma nonlinearities to increase the bandwidth of the pulse. Two copropagating laser beams with a near resonant detuning, that is they have a difference in frequency near the plasma frequency, are sent into a plasma. This results in a periodic variation of index of refraction in time which will cause a movement of energy to different frequencies. A coherent electromagnetic (EM) cascade occurs with energy being concentrated into a train of pulses with a period equal to the beat period (the period corresponding to the beat frequency between the incident pulses). The overall result is to increase the bandwidth and then compress the new frequencies into a higher peak power using nonlinearities. Two different plasmas can be used. One as a Modulator and one as a Compressor. The first is of low density and yields frequency modulation. The second is of high density with a corresponding Group Velocity Dispersion (GVD) and yields a compression of the frequencies from the Modulator.

Simulations at UT Austin were done by Kalmykov for the Chirped Pulse Raman Shifter that we have developed. The results are shown below. Notice the roughly octave spanning output frequency spectrum. An exciting five times increase in power is predicted. This is one future area of research for our group.

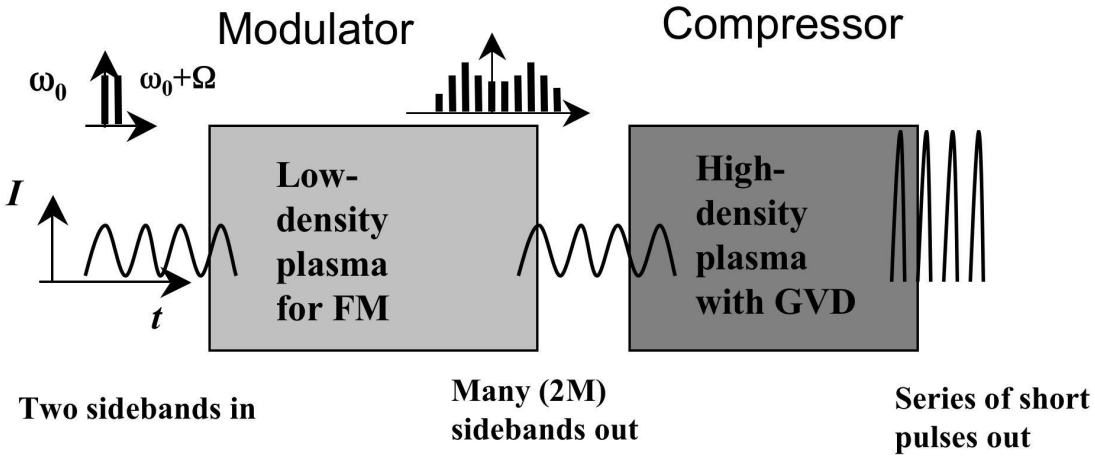

Figure 1.3: Schematic that shows a two-stage EM cascade compressor

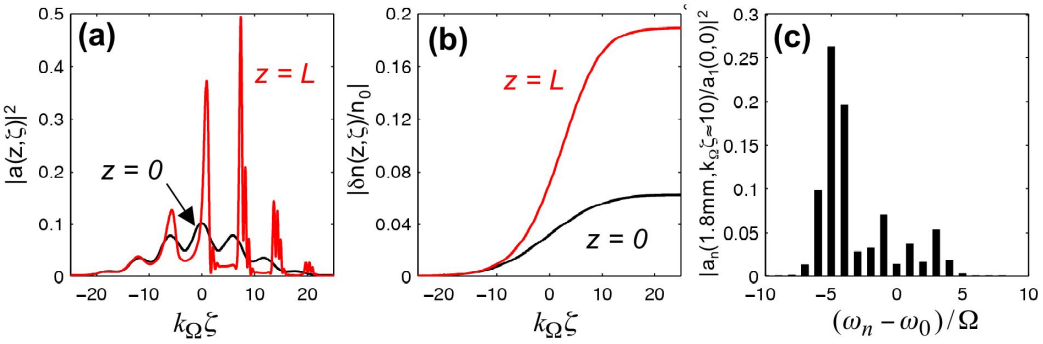

Figure 1.4: 1D simulation of a EM cascade using the barium nitrate Raman shifter and a 800 nm pulse. a) the pulse evolution as it propagates through the plasma b) the plasma response c) the pulse spectrum at output. The difference in frequency is 0.95 ω_p. The beatwave is downshifted by 5 percent. Electron density is 1.35x10^{19} cm^{-3}.

1.4 Conclusion

A two color high intensity laser source is highly desirable for studying new physics and for more easily and accurately advancing currents experiments (for instance use of a low group velocity walkoff probe). Experiments such as Raman seeding of the laser wakefield using a two color source allows coherent control of a high intensity process and higher accelerated energies to be achieved. Raman cascade in plasma using a two color source allows a very large broadband source at high power to be achieve. Subsequent compression in plasma of the Raman cascade allows large increases in power. Future lasers at the limit of material damage threshold could use such Raman cascade and compression to achieve record powers to move past the damage limit of the optics in the laser chain. Experimental demonstration of the technique would be a significant advance in to the possible state of the art of high power lasers and motivates the construction of a two color high intensity laser source. Overall, many new experiments are possible with such a two color source, which has previously not been possible, of which RS-LWFA and Raman beatnote are two of the most exciting.

Chapter 2

Method for Realizing a Two Color Source at High Intensities

2.1 Introduction

Possible methods for generating a two color source are discussed in this chapter. Benefits of using Stimulated Raman Scattering and also Four Wave Mixing are outlined. Limitations for such methods using ultrashort pulses are outlined. Shifting of chirped pulses for high energies is shown to be desirable. An novel shifter and its properties is described and its significant advances to the state of the art are stated.

Given the need for a two color laser source with the colors not too far separated in wavelength, a practical source is needed. An additional laser oscillator tuned to a secondary wavelength could be constructed, but this will suffer issues of synchronization. A simpler method would be to shift some of the light in a CPA system. This allows modification of an existing system for two color experiments. Of the known methods for producing a modest 10 percent wavelength shift, Raman scattering and optical parametric processes are best known. One may suggest using a three wave parametric process for producing small wavelength shifts. However,

the idler wave produced in the infrared will tend to be absorbed by the IR cutoff. This generally prevents optical parametric processes from being used at the wavelength of our CPA system 800 nm. Stimulated Raman scattering can have high efficiency. In fact the quantum efficiency, can be close to unity. A suitable material must be used that has a high optical quality. A highly focusable beam is needed for RS-LWFA and other applications, so wavefront quality must be very good.

Previous work by Zhavoronkov [4] in the Raman shifting of chirped pulses provides a good starting point. Zhavoronkov et al. converted an 800 nm CPA system to an 873 nm wavelength. Microjoule energies of a single color were achieved. Here our goal is millijoule energies with a combined two color system. A pulse duration of roughly 200 fs, far from the transform limit, was achieved by Zhavoronkov. The source of poor compression was unknown. The goal here is to compress as close to the transform limit as possible (see appendix C for derivation of this limit). A novel compressor solution was sought out. A beam with significant deviations from Gaussian mode was made previously. Here a mode suitable for tight focusing for high intensity work is sought. Significant gains to the state of the art are sought in the work presented here.

2.2 Raman Active Mediums and Initial Attempts at SRS of Chirped Laser Pulses

Hydrogen is a well known Raman shifter with many good properties. However, it produces a shift of about 400 nm from an initial wavelength of 800 nm. A solid state crystal with high gain is Barium Nitrate. $Ba(N0_3)_2$ is produced in large enough optical quality sizes, typically 1 cm x 1 cm x 5 cm long is available. Comparing barium nitrate to hydrogen, see the figure below for the gain at different wavelengths. Barium nitrate has a much higher gain which leads to a more compact apparatus.

Ultimately, Barium Nitrate proved most appealing because of its high gain, the wavelength shift was just about perfect as it was outside of the bandwidth of a standard Ti:sapph CPA system, FWHM = 20-30 nm, and it was available in large optically flat high quality crystals.

The compressed fs pulses from the CPA system can not be Raman shifted. The fs pulses will produce self-phase modulation in barium nitrate. Also, the gain will be very low as the pulse length of order 100 fs, is much smaller than the characteristic time for Raman scattering to occur which is typically tens of ps. For barium nitrate, T_2 is 25 ps. To get around these problems, we will shift the chirped pulses in the middle of the CPA chain. The advantage of this is that the shifted pulses are perfectly ready to be amplified. This makes this technique highly general and allows for very high power two and even three or more color systems possible.

As an aside, is it possible to amplify (for an overall gain factor of 2-10) the compressed Stokes beam (obtained by methods detailed below) in Barium Nitrate by transient SRS with the pump? Problems include self-phase modulation, group velocity walkoff, and low gain. The possibility of generating a very broadband source of radiation is exciting, but practical problems likely prevent its realization in the laboratory. An interesting followup experiment would be to look at impulsively excited Raman scattering in a multi-pump pulse experiment where a delayed fs pulse scatters off the material wave generated by the intense primary pulse. The experiment has been done in Hydrogen, but it would be new to do it in a solid state medium. For very short pulses, the oscillation of molecules in Barium Nitrate with a 31.83 fs period would create a sinusoidal modulation of the decay of the material wave, if the Hydrogen work can be extended to Barium Nitrate, that could be used to phase modulate the weak delayed pulse. Ultimately, a plasma may be the best medium for short pulse Raman scattering. A Raman cascade with

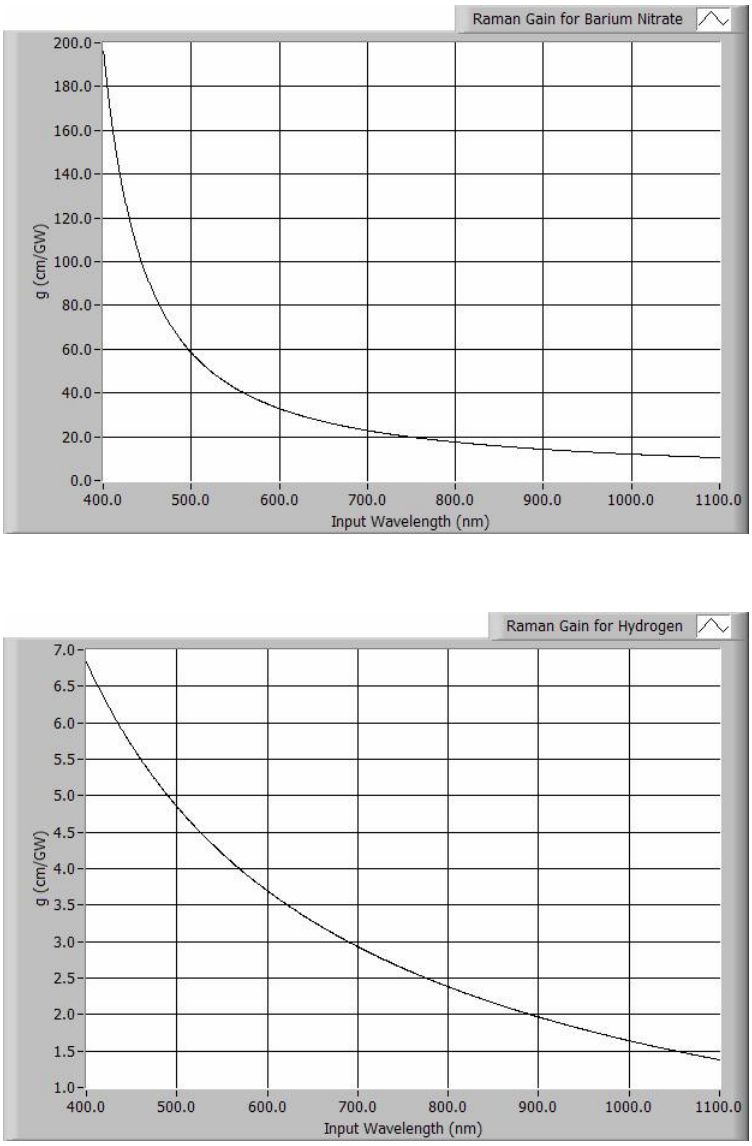

Figure 2.1: Plots made in Labview with Raman Gain vs Wavelength Plotter.vi.

subsequent plasma compression is an exciting high energy method of generating broad bandwidth fs radiation source.

As a first attempt, the Barium Nitrate crystal was placed in the pre-amplifier beam with the energy of the pre-amp beam adjusted so that the energy of the beam would be above threshold for Chirped Pulse Raman Scattering (CPRS), but below damage threshold for this uncoated crystal. A fluence in excess of 1 J/cm^2 was incident. Poor beam quality was achieved with modest efficiencies, see Figure 2.2. Initially, the 800 nm beam was sent through the Barium Nitrate crystal and an Ocean Optics S2000 fiber spectrometer was used to search for light at the 873 nm sideband. The power here is larger than the critcal power for self-focusing. However, the B integral was only around one. Overall, nothing could be done to improve Stokes beam quality. Changes in the incident beam, for instance attempting to improve its quality, did not make a difference. Another scheme was ultimately hit upon through trial and error that worked.

The two main hurdles encountered in scaling CPRA from microjoule [4] to millijoule output energy are: 1) onset of filamentation; and 2) competition between first Stokes and higher-order Raman amplification. The first issue limits output energy of the first (SRS) stage to 0.1 mJ. Below this threshold, a high quality Gaussian mode can be achieved. Attempts to extract higher energy result in a filamented beam of limited usefulness, as shown in Fig. 2.2(a). Twenty percent conversion (1 mJ) to 1st Stokes is possible, but only with a pump that exceeds the critical power for self-focusing. In normal operation, we restrict first stage output to 15μJ, in order to completely eliminate filamentation.

2.2.1 Calculation of Self-focusing in Barium Nitrate

There is an issue of whether self focusing can occur in the barium nitrate crystal near the threshold for observation of Raman shift of 1.2 GW/cm^2. Self focusing

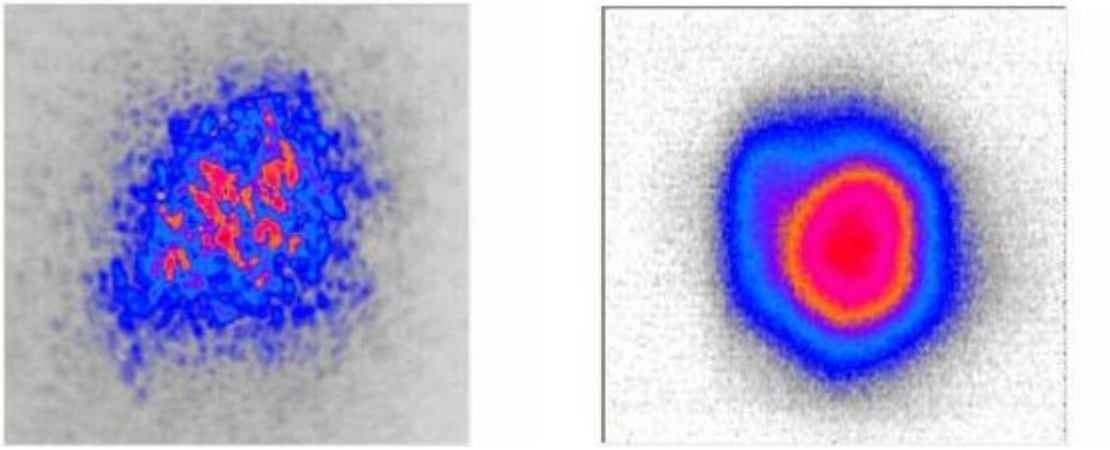

Figure 2.2: (a) Transverse profile of first Stokes beam produced by single pass stimulated Raman amplification to 1 mJ energy, showing filamentation. (b) Profile of first Stokes beam of similar energy produced by seeded Raman amplification in second stage, showing nearly Gaussian mode. Pump intensity is much lower in the seeded amplifier.

can lead to damage and to irregularities in the spatial phase of the beam. The rough dependence of the focal length is $f \sim w^2/E$. However, using the formula, $f \sim w_o^2/(((P/Po)^{0.5} - 0.852)^2 - 0.0219)^{0.5}$, where P_o is the critical power for self-focusing, gives a focal length for a 1 mJ, 800 nm, duration 200 ps, and a 1.2 GW/cm^2 intensity of 24.5 cm. A more recent measurement of n_2 for barium nitrate gives a n_2 of 7.1x10^{-16} cm^2/W [8]. The focal length from n_2 is longer than the crystal length of 5 cm. Measurable self-focusing of the seed beam was not observed.

2.3 The Chirped Pulse Raman Amplifier (CPRA)

Higher first Stokes energy is then achieved by seeding a second Raman amplification stage with the high quality output mode of the first stage. This re-initiates Raman amplification with the non-filamented second-stage pump. The mode quality of the first stage output is then preserved through amplification to millijoule energies in the

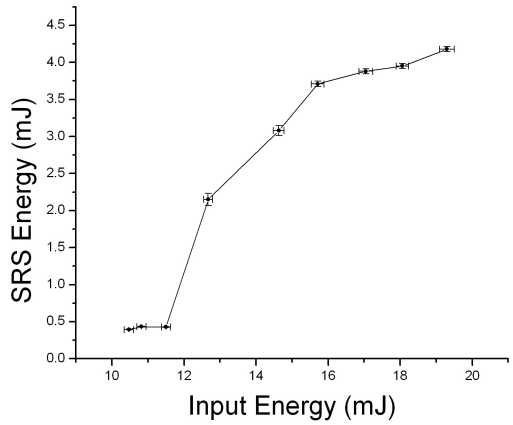

Figure 2.3: Stokes beam energy out of the seeded second-stage, two-pass Raman amplifier as a function of the second-stage pump energy.

second stage, as shown in Fig. 2.2(b) for energy 1 mJ. At this energy, Raman beam cleanup the amplified Stokes beam assumes the pump beam profile with smoothed irregularities. For example, the feature in the upper left corner of the profile in Fig. 2.2(b) was transferred from the pump, where it was much more prominent. To maintain good beam quality, overall gain in the seeded second stage amplifier was kept to 300. Because a seed was injected, pump intensity could be kept below the level required for single-pass Raman amplification to the same energy, thus preventing filamentation.

The second issue sets the primary limit on Raman gain in the second stage. Higher order Raman processes (*e.g.* four-wave mixing) become important when the peak intensity of the growing Stokes pulse becomes comparable to pump intensity. This can occur even when the Stokes pulse energy is only a few percent of the pump pulse energy, because the most intense parts of the Stokes pulse experience preferential

SRS gain. These competing processes deplete both first Stokes and pump energy, causing first Stokes gain to saturate well below the theoretical quantum efficiency (91.6%) of SRS. In order to manage these saturation effects, we divided the second stage amplifier into two passes. After the first pass, the first Stokes component of the incipient Raman cascade is spectrally and spatially filtered, then preferentially seeds second-pass Raman gain. In this manner, first Stokes gain saturates at a higher level than for a single pass through a crystal twice as long. Figure 4 shows typical Raman gain saturation for the complete two-stage Raman amplifier. Second stage gain is observed above a threshold pump energy $\sim$ 12 mJ. Saturation becomes significant above $\sim$ 16 mJ pump energy, indicating that the amplifier is approaching optimum efficiency. Uncompressed Stokes pulse energy of 6 mJ is routinely achieved with pump energy of 20 to 25 mJ, sufficient for GW compressed power and 10^{16} W/cm^2 focused intensity.

As the first Stokes energy exceeds $\sim$1 mJ, and four wave mixing contributes increasingly to amplification, the mode quality typically degrades somewhat from the optimum near-Gaussian profile shown in Fig. 2.2(b). Nevertheless, it remains very good, focusable, and adequate for two color high intensity experiments.

Figure 2.4 showing the CPRA presents an overview showing how the Raman shifter and amplifier is incorporated into, and temporally synchronized with, the overall Ti:Sapphire CPA system. An amplified stretched laser pulse (wavelength $\lambda = 800$nm, duration $\tau = 200$ps, energy $E = 180$mJ, repetition rate 10 Hz) from an intermediate amplifier stage of the Ti:Sapphire CPA system is split into two pulses with intensity ratio 15:85. The weaker pulse ($\sim$30 mJ) is Raman shifted to 873 nm with 6 mJ energy, then compressed by a dedicated 873 nm compressor (830.8 lines/mm gratings) to 115 fs. The stronger pulse ($\sim$150 mJ) is further amplified to 500 mJ, then sent to an 800 nm compressor (1200 lines/mm gratings) and compressed to 90fs. Both pulses are combined by a dichroic mirror and sent to the

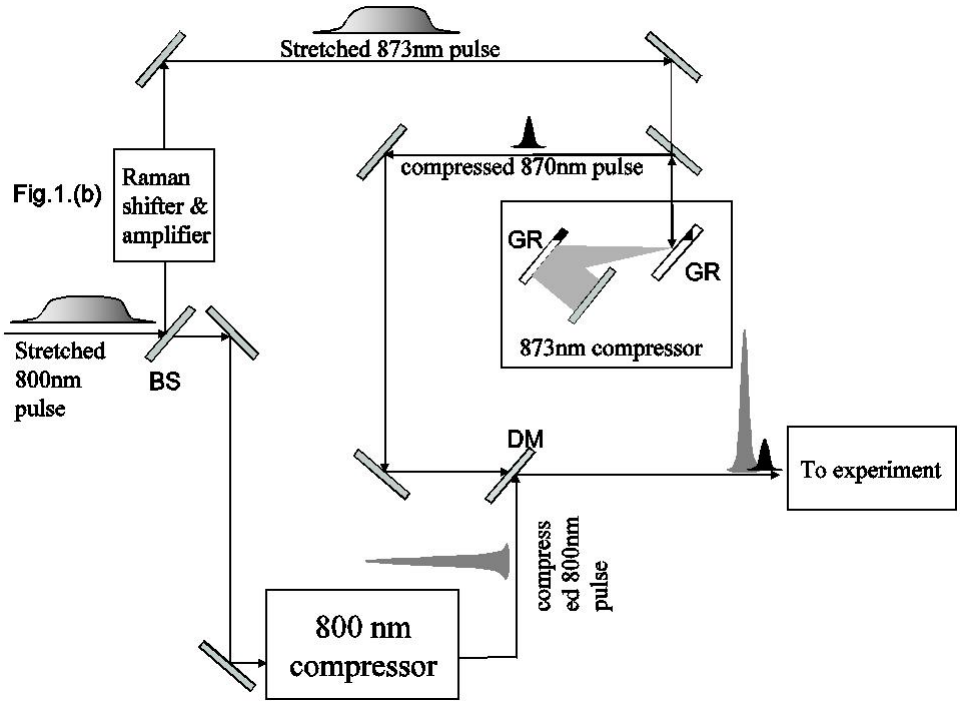

Figure 2.4: Overview showing synchronization of Raman amplifier with 800nm Ti:S amplifier output. BS=beam splitter, DM=dichroic mirror, GR=grating.

experimental chamber.

Figure 2.5 shows detail of the Raman shifter and amplifier. The incident 800 nm pump beam is split in the approximate ratio 1:100. After the beam splitter, the weaker portion (300μJ) is focused at f/20 into a $Ba(NO_3)_2$ crystal to generate an 873 nm first Stokes seed, primarily by SRS. Crystal position is adjusted longitudinally to optimize gain and Stokes beam quality. The $Ba(NO_3)_2$ crystal, purchased from Marketech International Inc., was 5 cm long, 1 cm $\times$ 1 cm cross section, and had uncoated end faces normal to the pump and seed beams. $Ba(NO_3)_2$ is used because of its high gain coefficient in the stationary regime. Because the Raman mode dephasing time T_2 = 25 ps in $Ba(NO_3)_2$, SRS shows characteristics of the semi-transient regime in our system. [4]

The remaining 99% of the pump pulse (30 mJ) passes through a delay line to synchronize its arrival at the second stage with the 873 nm seed pulse. Figure 2.6 shows the energy of the Stokes beam as the delay is varied. There are multiple peaks. The CPRA is a saturated amplifier so weak secondary pulses are being amplified. Normally, they can not be detected in the middle of the CPA chain. There is also a long tail in figure 2.6 which we believe to come from the long tail to the SRS linewidth in barium nitrate. This tail makes alignment somewhat easy as a SRS beam is produced even for significant offsets to the optimal delay. The pump and seed pulse pass through the second identical $Ba(NO_3)_2$ crystal twice at an appropriate phase-matching angle (discussed further below). Phase-matching is more important in the second stage than in the first because of the greater importance of four-wave mixing (4WM) relative to SRS in the amplification process. Normally four wave mixing is seen in a collinear SRS setup after saturation of the gain for the Stokes beam. Rings of higher Stokes and anti-Stokes light are emitted with the angles set by phase matching in the material. By adjustment of the angle between the incident pump and 1st Stokes beam, the phase matching can be changed. However, an additional benefit of the angle is that in the non-collinear geometry, beamsplitters are not necessary to separate out the Stokes beam. The setup is therefore simplified and no Stokes energy is lost in the beamsplitters. The amplified 873 nm pulse is then sent to its custom-designed compressor.

As 4WM increasingly dominates second-stage amplification, a cascade of higher-order Raman lines can be observed after each pass when the angle between pump and incident seed beams is optimized to yield highest overall energy. A photograph of the Raman cascade viewed on a fluorescing screen following the first pass of the second-stage, taken with a Canon A75 digital camera is shown at the top of Fig. 2.5. The cascade consists of first (873 nm) and second (961 nm) Stokes, and first (738 nm), second (685 nm) and third (639 nm) anti-Stokes radiation. The

various wavelengths are spectrally dispersed at angles determined by phase matching in the crystal. Such cascades were not observed from the first stage, nor in previous work[4]. In the normal operation reported here, the pump-seed intersection angles in both stages and the reflectivity spectra of the amplifier mirrors are chosen to optimize the first Stokes output. However, any of the other Stokes or anti-Stokes beams shown in Fig. 2.5 could be individually optimized and compressed in a similar manner. Therefore, it is possible in principle to compress the entire cascade to synthesize attosecond pulses.[14]

As an example of the effects of seeding a Raman process, take a historical example, the seeding of a Raman process with a laser diode. As was seen, the laser diode seed serves to stabilize the Raman process. It effectively transforms it from an instability to a stable amplifier. In the work of Wessel et al.[9], a Raman amplifier was seeded with a visible laser diode in order to stabilize the amplifier output. It was found that the energy, spectrum, and spatial characteristics were stabilized compared to the unseeded case. When the amplifier was unseeded, the beam would grow from spontaneous scattering or noise photons.

Barium Nitrate was the material seriously considered for SRS at UT Austin because of it's high gain and it's n_2 was not too high. However, it is interesting to note that there are a wide range of solids, liquids, and gasses suitable for SRS. Overall the CPRA technique allows current CPA systems to access almost any optical wavelength.

Stimulated Raman scattering is not a phase matched process when you consider a single plane wave incident on a crystal. However, when multiple wave vectors are present as in any real beam, the interaction becomes more complicated. The process of Raman beam cleanup, well known in the literature, can occur due to a convolution of the pump and seed fields as they go through the crystal [7]. Raman

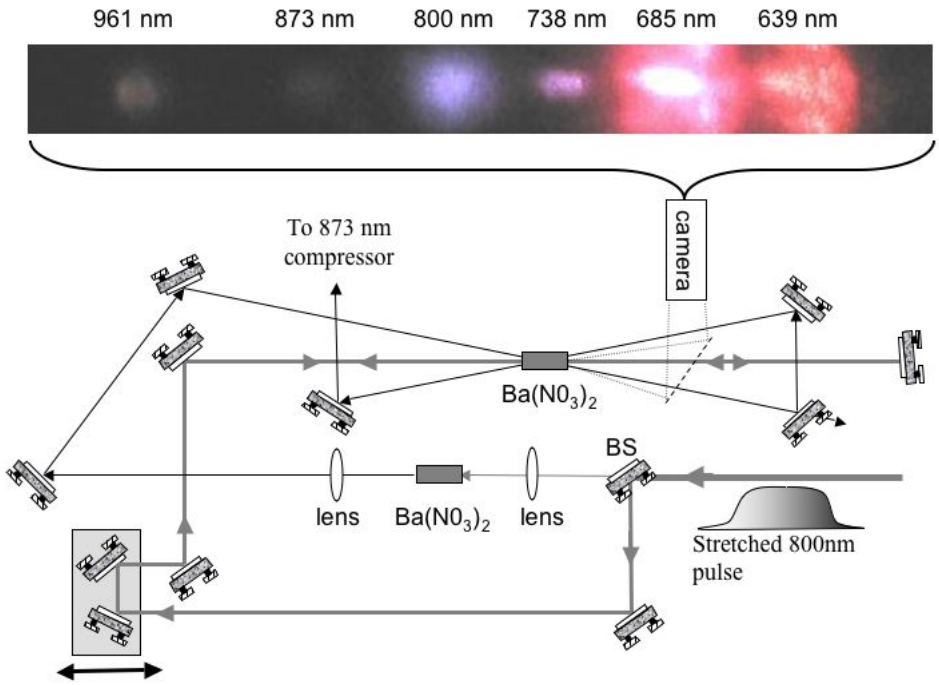

Figure 2.5: Details of stimulated Raman shifter and two-pass Raman amplifier. Top: photograph of Raman cascade output of first pass of Raman amplifier, with intersection angle of pump and seed adjusted to optimize phase matching. Relative intensities in the photograph are determined by fluoresce efficiency of the screen (dashed line) and detection efficiency of the camera, and do not indicate relative intensities emerging from the crystal. The screen is removed in normal operation.

beam cleanup enhances the CPRA as it provides an improvement in the mode.

Equations for Raman Beam Cleanup:

$$\vec{P_s}(r,z) = \chi_{Rs} : |\vec{E_s}(r,z)|^2 \vec{E_p}(r,z)$$

which is equivalent to in k space:

$$\vec{P_s}(k,z) = \chi_{Rs} : \int \mathrm{d}k \vec{E_p}(k,z) * * \vec{E_s^*}(k,z) * * \vec{E_s}(k,z) e^{-ikr}$$

Notice now that a phase mismatch term will arise from the convolution and will cause an evolution in the beam as it goes through the crystal. However, a poor quality, unfocusable output can occur if real beams with non gaussian quality and a source of noise are used to seed the interaction. But for well behaved initial beams, a smoother output Stokes beam is expected. To understand better how Raman cleanup can occur, let us examine the nature of convolution as it affects another optical process, diffraction. It is well known that in the far field, the diffracted field is given by the fourier transform of the light at an initial plane. If there is a mask at that plane, such that the field there E*=E*M where M is the mask function, then in the far field the field will be the convolution of the transforms of E and M. For a M which is an aperture, a step function, the transform will be a sinc function. The effect of convolution in the far field with the smooth sinc function will be to average out the features of the transform of E. For a rough initial far field pattern, if the aperture is closed sufficiently that the sinc function half max width is greater than the feature size, then the far field pattern will become smoothed out. We can see then that the convolution process will yield a smoothing out of rough features.

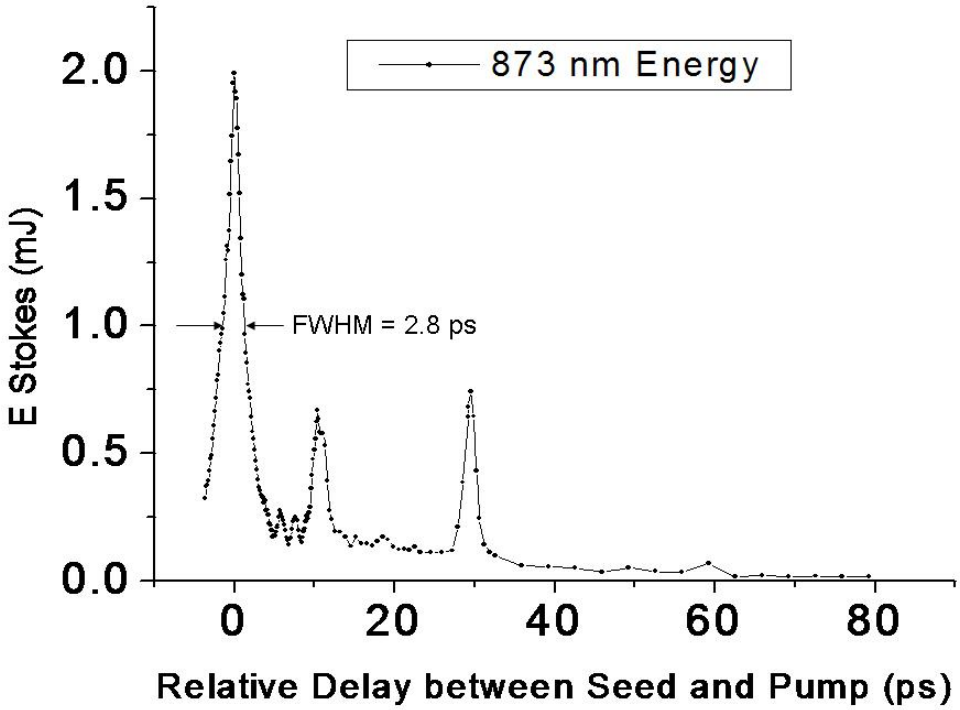

Figure 2.6: Stokes energy versus delay between Stokes beam and pump beam. Note that the central peak has a width given by the linewidth of the transition taking into account gain broadening. The secondary peaks are from secondary pulses and the long tail is from the spectral tail in the Raman gain.

Determination of the intensity of the pump beam in the Raman generation process relies on accurate measurement of the pump duration. A technique not commonly cited in the literature was used here. In a background free geometry, the chirped pulses were SHG autocorrelated with a BBO crystal with a phase matching bandwidth was larger than the bandwidth of the pulse. The crystal was thick enough to give a strong signal that was measured with a Molectron energy meter head. The resolution is limited by the angle used which was small. This technique does not require the use of expensive fast photodiodes and can give a sub-ps resolution. The pulse duration measured agrees with ZEMAX ray-trace simulations to within 1 percent.

2.4 Mismatched Grating Compressor Design for Near Transform Limited Pulse Duration

The chirp of the pump CPA pulse is transferred to the CPRA pulse. However, the CPRA pulse is poorly compressed with gratings matched to those in the main pulse stretcher and compressor[4]. This is because the Stokes shift breaks the symmetry between stretching and compression mechanisms. The material in the laser chain also breaks this symmetry. As has been previously shown, large higher order residual dispersion can be compensated by mismatched gratings in stretcher and compressor[13]. Figure 2.7 shows the compressed 1st Stokes pulse for our system calculated from a model of our laser/Raman amplifier system with optimized 1200 line/mm compressor gratings, using the ray-tracing program ZEMAX and a Fourier transform routine. The compressed 1st Stokes pulse shows strong residual asymmetric chirp, and a pre-pulse train extending over ~ 1 ps.

Good compression of the CPRA pulse requires gratings mismatched to those used in the main pulse compressor and stretcher. We investigated alternative 1st Stokes compressors using ZEMAX, focusing on commercially available gratings that could be made large enough to be useful in a high energy system. For each line density, grating separation and beam angle were adjusted to optimize compression with group-velocity dispersion (GVD) and third-order dispersion (TOD) zeroed. Residual fourth-order-dispersion (FOD) could be minimized by further compressor adjustments, but was correlated closely with FOD of the main pulse. When the latter was zeroed, compressed 1st Stokes pulses as short as 45 fs FWHM were calculated, assuming frequency bandwidth of 20 nm FWHM. In practice, residual FOD in the main pulses limited 1st Stokes pulses to longer durations, as illustrated by the calculated 20 nm bandwidth, 60 fs FWHM profile in Figure 2.7, compressed with 830.8 line/mm gratings. The asymmetric pre-pulse train is eliminated and peak power improved five-fold compared to compression with matched gratings (Fig. 2.7).

Based on this model, we constructed a CPRA compressor using 830.8 line/mm gratings purchased from Richardson Grating Laboratory. The 830.8 line/mm compressor gratings had a separation of about 225.6 cm, optimized in situ, and angle of 53.0 degrees. Fig. 2.7 shows an experimental single-shot autocorrelation of an CPRA pulse corresponding to a temporal FWHM of 115 fs assuming sech. The discrepancy with the calculation in Fig. 2.7 results from limitation of the bandwidth to 9 nm limited in part by optics that cut off part of the bandwidth. Nevertheless, even with these shortcomings, the compression is vastly improved compared to previous results with matched gratings.[4]

The unseeded CPRA pulse was also attempted to be compressed, but it yielded very poor compression. This initial attempt was based on a very rudimentary idea of compression with existing 1800 line/mm gratings. It is clear now that this scheme could not work. However, even this weak beam yielded autocorrelation output which was measurable.

2.5 Focused intensity

Figure 2.8(a) shows images of the spot profile of the CPRA (873 nm) and main (800 nm) pulses in vacuum after focusing by an f/6 off-axis parabolic mirror. The two pulses focus to very similar spot sizes and shapes (Strehl ratio xxx), confirming that the profile of the pump pulse is transferred to the CPRA pulse with high fidelity. In vacuum, the focused, compressed CPRA pulse reaches an estimated peak intensity 10^{16} W/cm^2 with 3 mJ energy. In air, the same pulse produces a bright ionization spark (Fig. 2.8b, center). After the spark, the pulse experiences plasma lens defocusing, and an ionization blueshift to visible red wavelengths, as shown in Fig. 2.8(b), right.

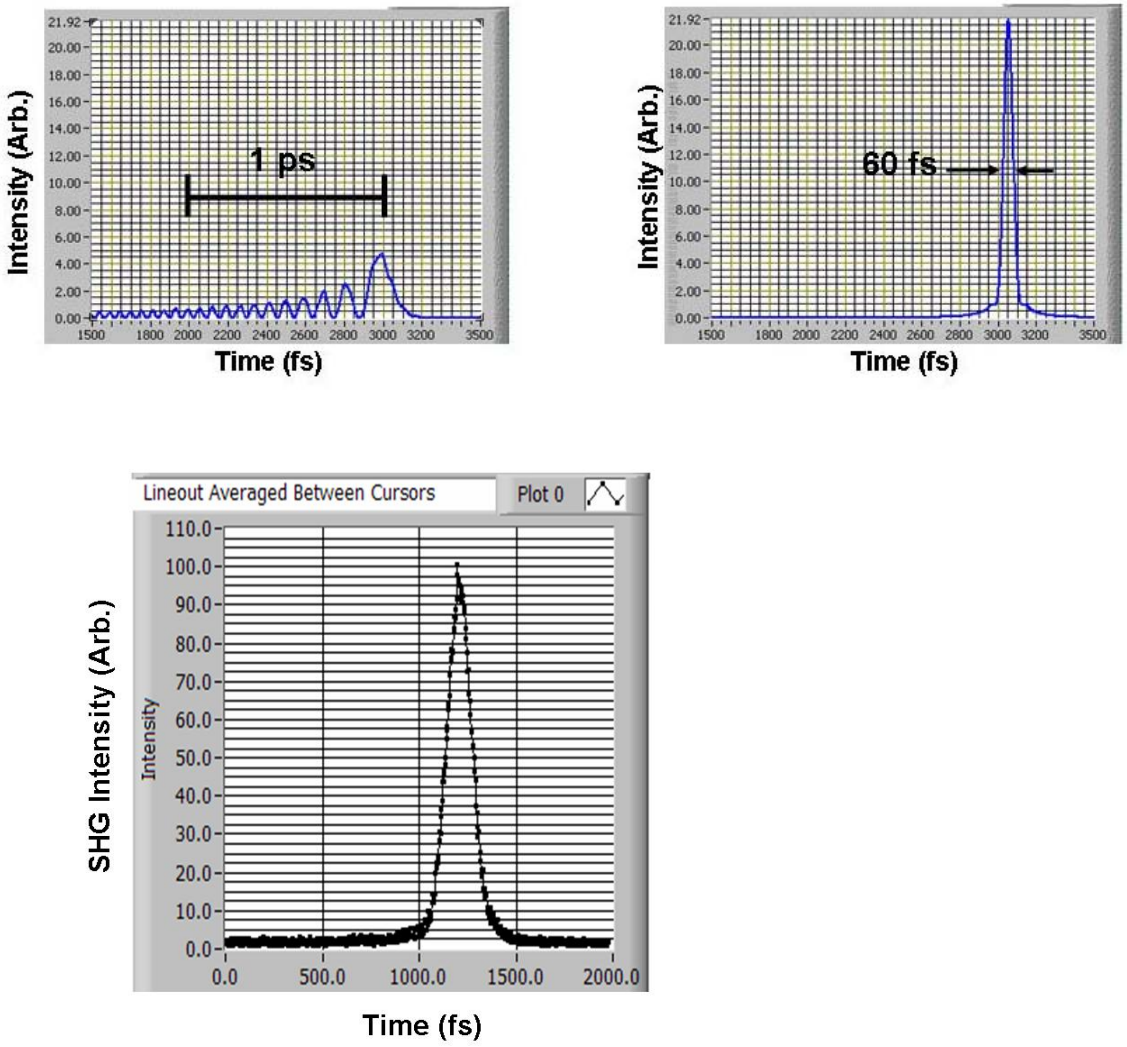

Figure 2.7: Temporal profiles of compressed 1st Stokes beam. (a) Profile calculated from a model of laser/Raman amplifier and optimized compressor with 1200 line/mm gratings, based on the ray-tracing program ZEMAX. (b) Similarly calculated profile, but with 830.8 line/mm compressor gratings (separation: 225.56 cm; angle: 52.97 degrees; Residual FOD: -1.9x10^6 fs^4, with 2.5x10^6 fs^4 in main pulse). (c) Measured single-shot, background-free SHG autocorrelation trace of 1st Stokes pulse from compressor with 830.8 line/mm gratings. Averaged pulse FWHM = 115 fs.

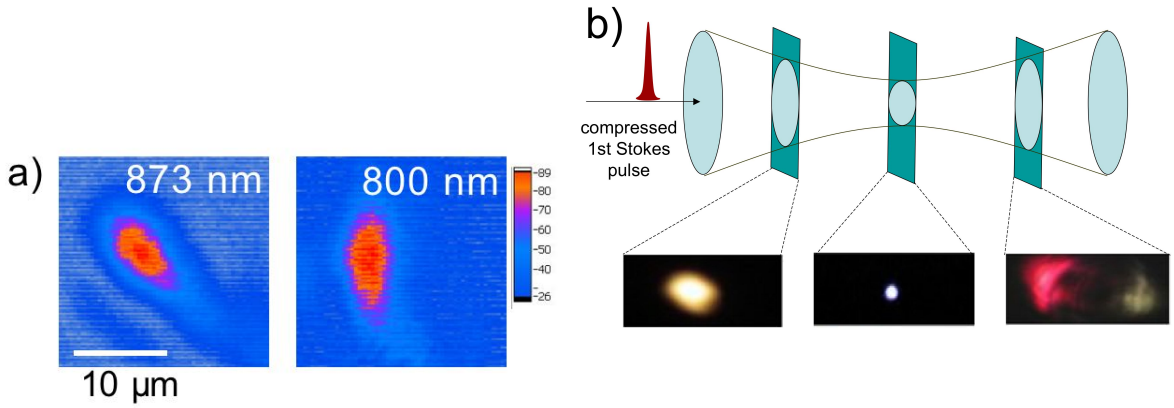

Figure 2.8: a)Intensity profiles of 1st Stokes and fundamental pulses at focus of f/6 parabola. b) Schematic, top, and digital photographs, bottom, showing the incident focused Stokes beam fluorescencing on a screen (left), the laser produced spark at focus (center), and the ionization defocused beam after the focus (right). Ionization blue shifted light from the IR Stokes beam is visible.

The focused mode of the CPRA beam is somewhat more gaussian than the pump mode even though part of the pump pre-power-amplifier was used to generate the CPRA beam. The pump has waists of 10.8 μm and 5.5μm in the x and y directions, respectively. The CPRA focused mode has waists of 6.7μm and 5.1μm in the respective directions with similar initial beam sizes. The CPRA unfocused beam is symmetric in the x and y directions. It is a significant achievement to get an amplifiable beam that greatly increases accessible bandwidth and still focuses tightly.

2.6 Synchronization with the Main Pulse and Phase Jitter

The main 800 nm pump pulse must be synchronized with the 873 nm Raman shifted pulse. Each has its own CPA line after the seed energy for the CPRA system is split off. The path lengths of the two lines must be the same to about a micron. In addition, any mechanical vibration or jitter in either line could cause a difference in the arrival time at target. A tape measure was used to measure the distance between all the elements of the 800 nm CPA system. The CPRA system was designed to be exactly as long up to the dichroic used right before the interaction chamber including a long delay line for synchronization. Because the pump pulse generates the CPRA pulse, the two pulse envelopes are automatically temporally synchronized, enabling two-color pump-probe experiments. Temporal overlap of the pulse envelopes was confirmed by generating their sum frequency in a KDP crystal. In addition, with the two pulses co-focused in air, and the 1st Stokes probe pulse attenuated below the threshold for self-ionization (see Fig. 6(b)), pump-induced defocusing of the 1st Stokes pulse was easily observed at positive pump-probe delays. The pump pulse first ionized air in the unevacuated interaction chamber. Sending the Stokes beam in with the pump, for timing where the Stokes arrives after the pump, defocusing of the Stokes after the focus is observed. The Stokes is separated out using dichroics and monitored. By looking for the point were such defocusing stops, the point of zero delay can be roughly found.

To find the point of actual zero delay, a more sensitive technique was used. Spectral overlap between the Stokes and pump was nonexistant as measured by a sensitive spectrometer. To create spectral overlap, a window mounted in a mirror mount was introduced after focus as in fig. 2.9 a). The glass created self-phase modulation which generated a white light as seen in fig. 2.9 b). The beam, containing both white light and Stokes light was sent to the spectrometer.

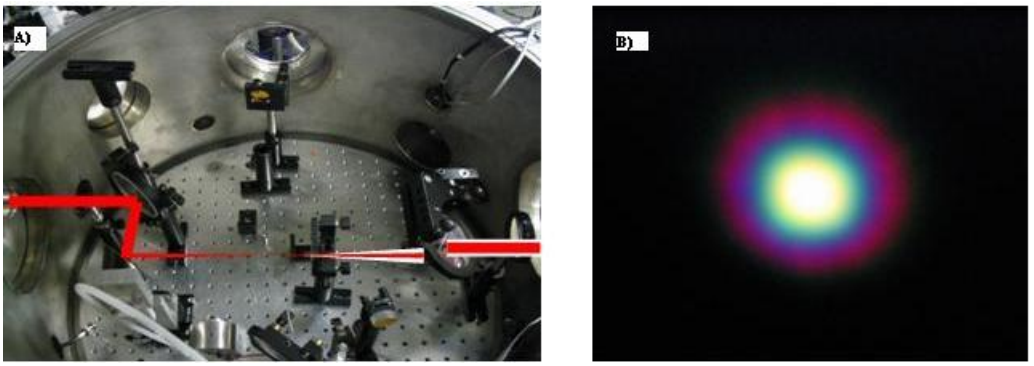

Figure 2.9: a) Experimental setup used to generated white light for spectral overlap. b) Digital camera picture of the white light generated by the 800 nm pump.

At the spectrometer, when the pulses where close together, fringes with separation inversely proportional to the time separation were visible. To see where such fringes come from, let us take two copies of the same pulse separated in time. The field is given by the following equation $E_{total}(t) = E(t) + E(t + \delta t)$. Taking the fourier transform of the equation, $E_{total}(\omega) = E(\omega) + E(\omega)e^{i2\pi\delta t\omega} = E(\omega)(1 + e^{i2\pi\delta t\omega})$. The magnitude squared of the field in time is the observed spectrum and you can see that a sinusoidal term (fringe) is produced: $I_{total}(\omega) = I(\omega)(2 + 2\cos(2\pi\delta t\omega))$. A band filter was used to look at light near 850 nm to 860 nm. As the micrometer was adjusted the fringe separation changed. A clear point was found where the fringes went away and the time separation was zero. See figures 2.10, 2.11, 2.12, and 2.13 for how the fringe separation varied with actual micrometer position. The white light generation process does not introduce a differential delay between pump and Stokes. Thus the zero delay point was found and the setup is ready for two color experiments.

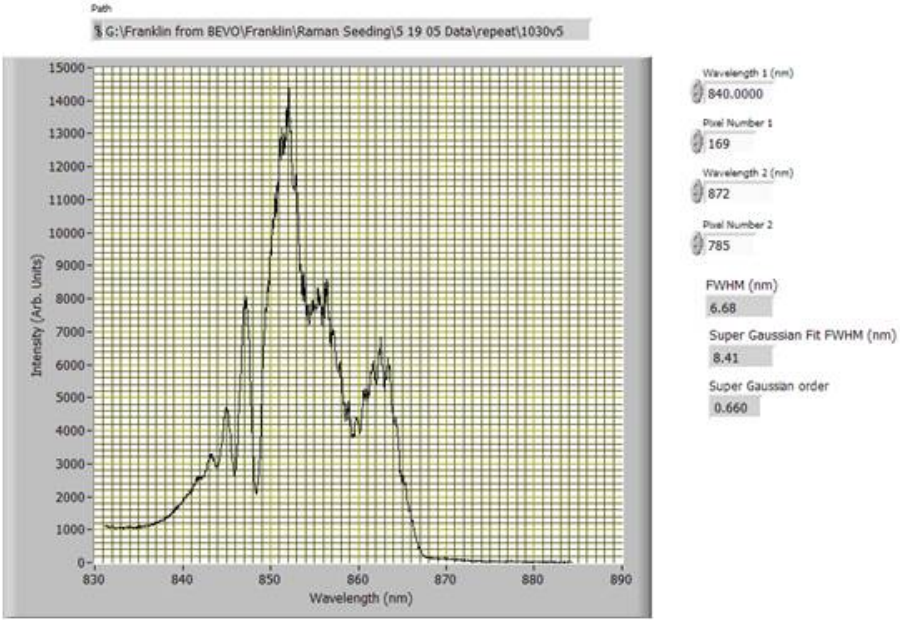

Figure 2.10: Snychronization interferogram of pump generated white light and 873 nm Stokes light at a micrometer position of 1.030 inches.

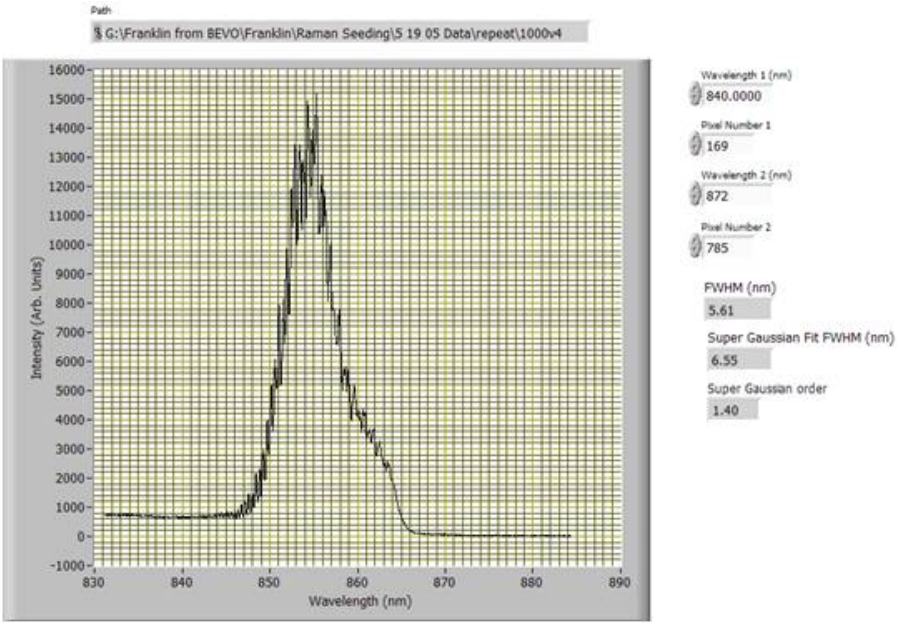

Figure 2.11: Snychronization interferogram of pump generated white light and 873 nm Stokes light at a micrometer position of 1.000 inches.

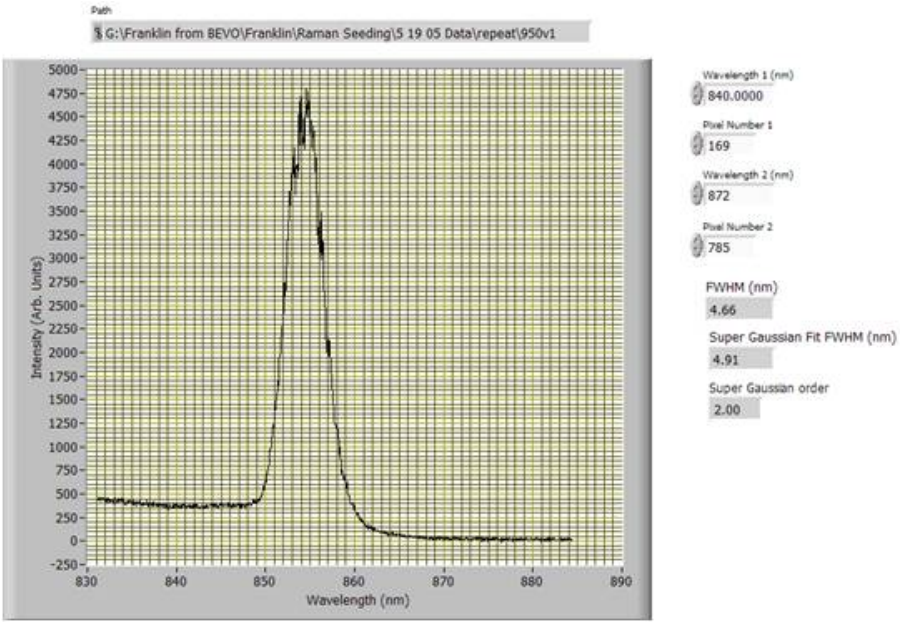

Figure 2.12: Snychronization interferogram of pump generated white light and 873 nm Stokes light at a micrometer position of 0.095 inches.

Phase jitter between the pump and 1st Stokes pulses is a more subtle question, because the Raman shifted pulse grows from spontaneous Raman scatter. The phase relationship between the Raman scattered beam and the fundamental is not determinate. As the SRS beam grows in intensity, the beam can rephase with the pump spatially. Also, when four wave mixing becomes appreciable, rephasing can also occur then as FWM is a phase matched process.

In order to determine whether a phase jitter was introduced into the Raman beam relative to the fundamental, two separate Raman seed lines were set up that each yielded few micro-joules of SRS light. The outputs of the two lines were synchronized and sent directly to a CCD camera with a slight angle between them.

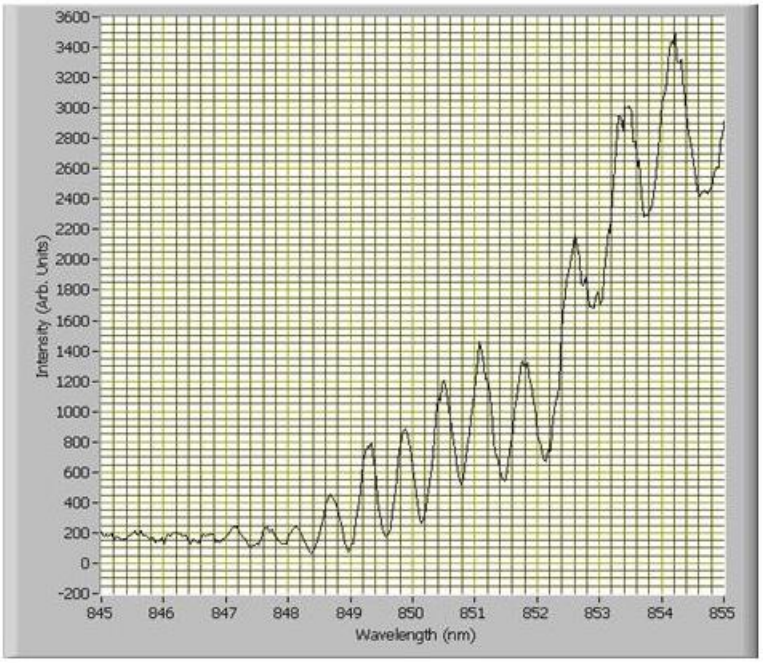

Figure 2.13: Zoom in of the spectral interferogram of pump and Stokes beams near synchronizaton in the overlap region between the white light from the pump and the tail of the Stokes spectrum showing the fringes. The fringe spacing is inversely proportional to the time separation between the pulses.

A series of interference fringes were seen. See figure below. The CCD camera data acquisition system was triggered by the laser system pulse trigger and successive shots were collected and later averaged to see if the fringes remained stationary from shot to shot. There were no moving parts in the optical apparatus. Colored filters, RG850 glass, were used to separate out the SRS beam from the much stronger pump. By removing the filters and translating one of the barium nitrate crystals slightly, the same experiment could be repeated with the pump beams for comparison. The interesting result of the experiment is that the SRS beams interferogram visibility quickly decreased with the number of shots averaged consistent with there being a random phase introduced to the beam in the Raman generation process.

For a random phase relationship between two beams in an interferometer, the visibility should drop to about 0.3 of its single shot value. The visibility of the 873 nm drop by about this factor indicating that a random phase is gained by the beam in the SRS conversion process.

Coupled equations for transient Raman scattering are given below. Note Δ is the difference in wave vectors between pump and Stokes and Δ_{-1} is the difference in wave vectors between pump and anti-Stokes. The coupled partial differential equations characterize the interaction through two orders of Stokes beams and one order of anti-Stokes beam. The material wave, q, is accounted for and is time dependent. Transient behavior is thus accounted for. Note that if you set the time derivative of q to zero, q can be solved for directly in terms of the fields. Also note that for positive $\frac{\partial q}{\partial t}$, q is reduced. For very short laser pulses in the transient

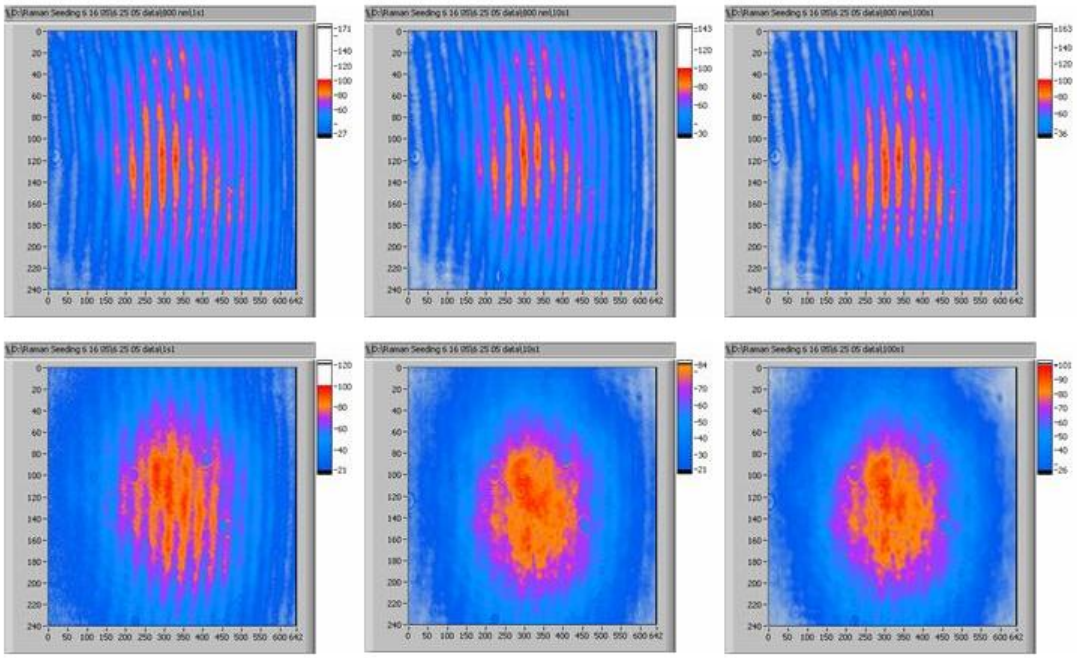

Figure 2.14: Top, CCD image of two beams interfering at an angle with averaging of 1,10, and 100 shots respectively from left to right. Bottom, CCD image of Stokes light from the same pump beams with RG850 colored glass filters inserted to filter out the pump light with averaging of 1,10, and 100 shots respectively from left to right. Note that the 873 nm fringes are only about 1/3 as visible after 10 shots indicating that a random phase is acquired in Stokes conversion.

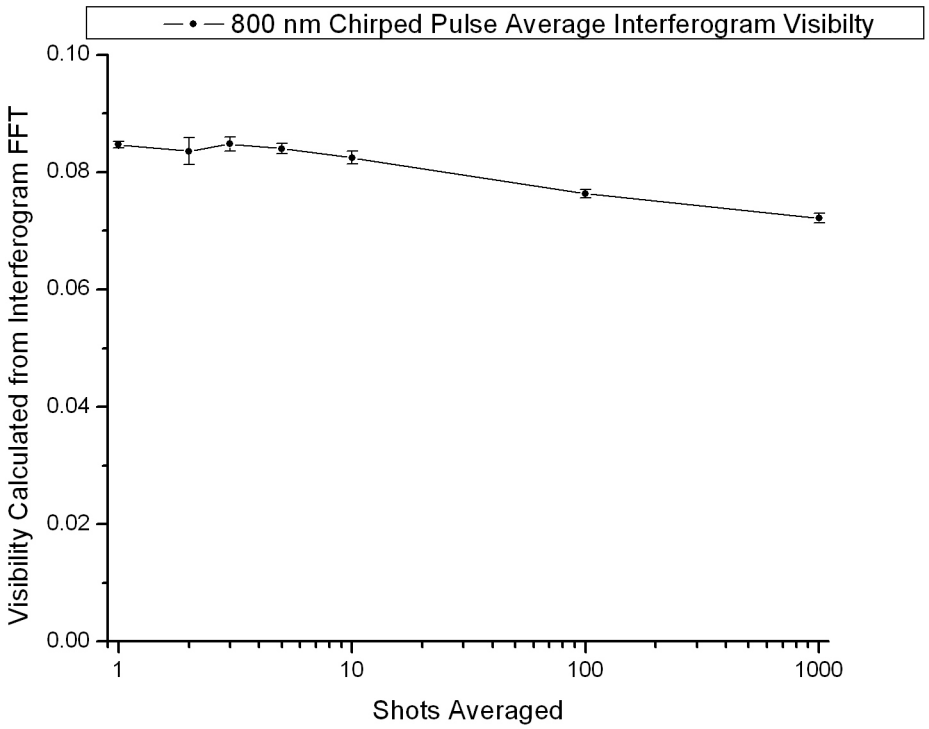

Figure 2.15: FFT measured visibility vs. consecutive shots averaged from 10 Hz laser for 800 nm pump beams. Note that the visibility is very stable and does not drastically decrease with the number of shots averaged.

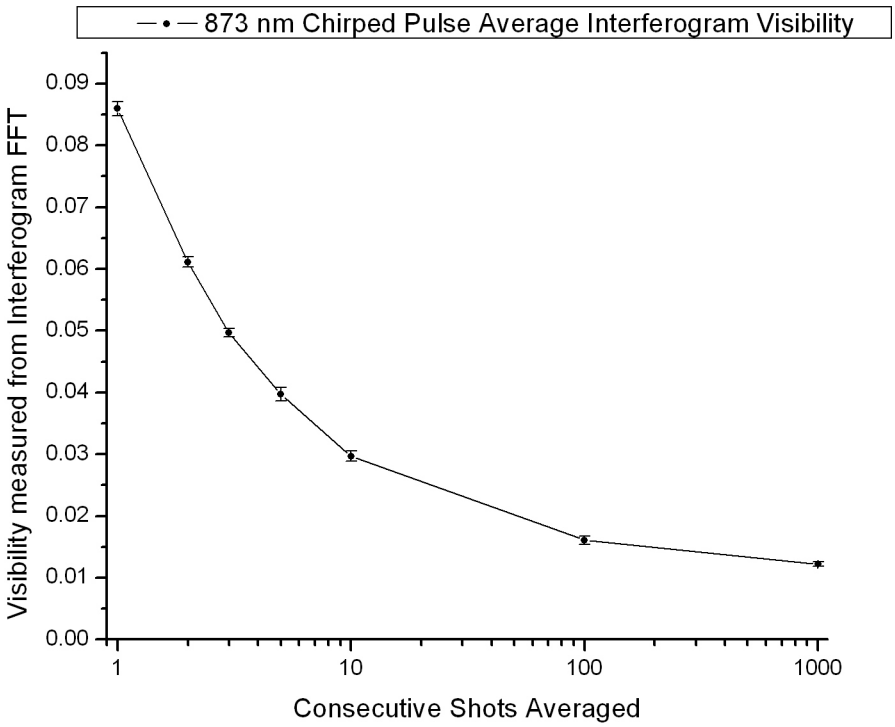

Figure 2.16: FFT measured visibility vs. consecutive shots averaged from 10 Hz laser for 873 nm Stokes beams. Note that the visibility drops off rapidly with the number of shots averaged indicating a random phase between the beams. RG850 has been inserted into the beam lines. No other change has been made to the apparatus. The change in visibility must come from the Raman generation process.

regime, SRS is suppressed. Our case of 200 ps pulses relative to the characteristic time $T_2 = 25$ ps for barium nitrate puts us in a regime where some transient effects can occur. It has been observed that the threshold for SRS for chirped pulses in this regime have a higher threshold intensity than in the stationary case[4].

$$\frac{\partial E_{2s}}{\partial z} = \frac{g}{2}\frac{\omega_{2s}}{\omega_s}E_s q^* e^{-iz\Delta_{-1}}$$

$$\frac{\partial E_s}{\partial z} = \frac{g}{2}[E_p q^* - E_{2s} q e^{iz\Delta_{-1}}]$$

$$\frac{\partial E_p}{\partial z} = \frac{g}{2}\frac{\omega_p}{\omega_s}[E_a q^* e^{-iz\Delta} - E_s q]$$

$$\frac{\partial E_a}{\partial z} = -\frac{g}{2}\frac{\omega_a}{\omega_s}E_p q e^{iz\Delta}$$

$$\frac{\partial q}{\partial t} = \frac{-q + E_s E_{2s}^* e^{-iz\Delta_{-1}} + E_p E_s^* + E_a E_p^* e^{-iz\Delta}}{T_2}$$

As an aside, barium nitrate has a relatively small linewidth which leads to a large Raman gain. Solution of these equations in the 1D limit was done using a split step method of solution programmed in National Instruments Labview. Four wave mixing was partially treated by accounting for the phase introduced by the angle between beams that is the angle appeared in the Δ terms. The solution exhibited features similar to what was found in the lab. As a characteristic example of the output, the energy yield for an angle where the second Stokes energy is higher than the Stokes is given in figure 2.17. When the angle was adjusted to be significantly larger than the 3 degree angle typically used for the CPRA, the second Stokes beam became more powerful.

However, ultimately, the threshold for SRS and the yields of the different Stokes and Anti-Stokes beams observed differed significantly from the simulation. However, the model was done in 1D because the solution in 2D is much more computationally complicated and was not attempted, but it would change the dynamics significantly.

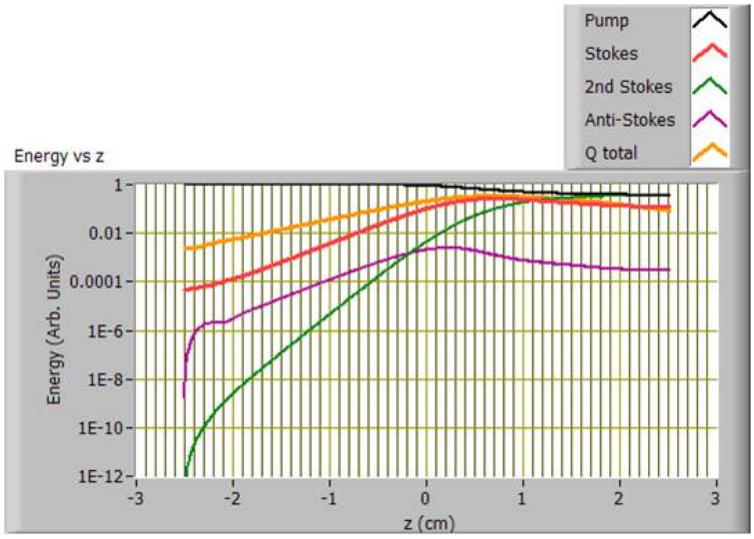

Figure 2.17: Simulated SRS beam energies as the pulses go through a 5 cm long barium nitrate crystal.

The intensity used in the 1D simulation was the peak intensity of the pump and seed on axis. The real beam has a spread of intensities off axis. Also, as was seen in the section on Raman beam cleanup, there is an interaction of different wavevectors for a real 2D beam. An area that is of future interest, is the 2D solution of the equations of the evolution of the SRS beams fully taking into account four wave mixing. Since it did not match experimental observation, the equations on the Stokes evolution are presented here to show the regime of transient SRS and to indicate future work that should be done.

For a Ti:Sapph laser at 800 nm, the wavelengths generated are given in the following graphs: figure 2.18 with a linear scale and with a log scale. Note the octave spanning wavelengths are possible. Also note that the same wavelengths would be produced in plasma by a RS-LWFA or a beatnote cascade using the CPRA as a seed.

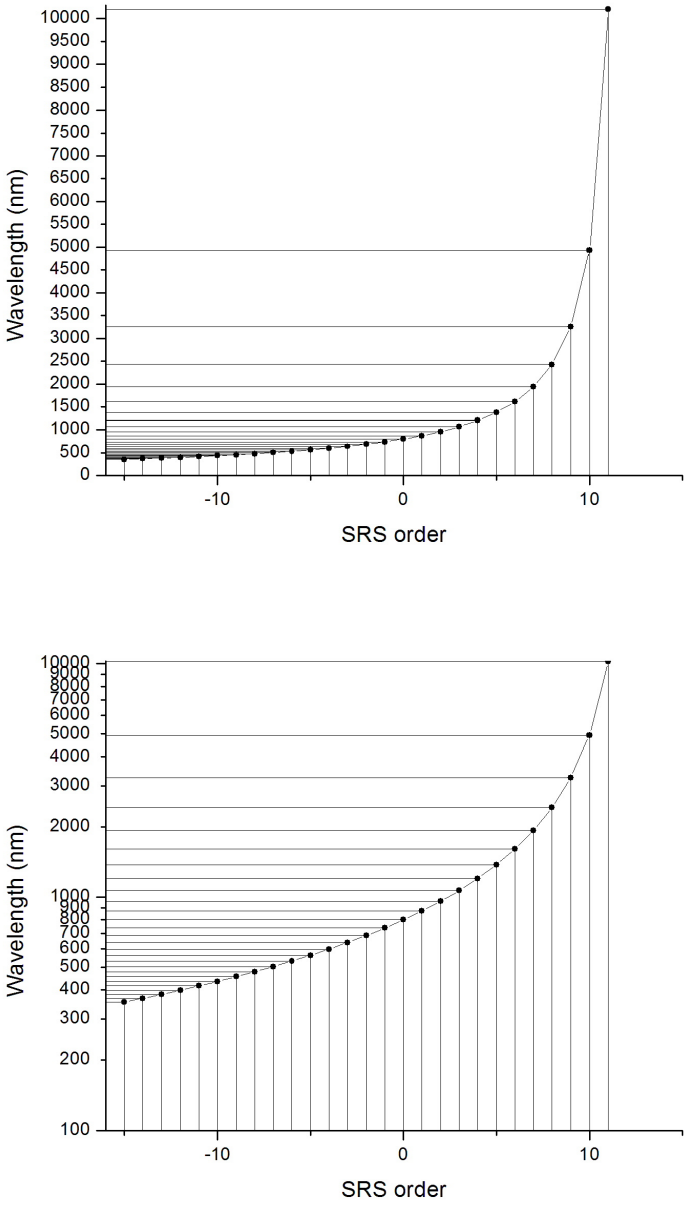

Figure 2.18: Raman Shifts in Barium Nitrate

2.7 Conclusion

A new Raman shifter for ultrashort TW scale lasers has been constructed. Shifted pulses just outside the bandwidth of the fundamental have been produced. The CPRA system is fully integratable into existing CPA systems, does not require pump lasers, and does not compromise the CPA system. A $M^2 \sim 1$ Gaussian beam quality was achieved. The beam has been focused for the first time and verified to be suitable for high intensity experiments. Fs temporal stability and synchronization was verified for the first time even over 20 m of delay difference between 800 nm and 873 nm CPA lines. Technical problems were overcome including filamentation of mJ level SRS beam which rendered the beam useless for high intensity experiments. A solution was found. A multi-stage non-collinear Raman amplifier was constructed that produces $M^2 \sim 1$ Gaussian beam quality. A micro-joule energy seed was generated by focusing a small portion of the energy in the middle of a barium nitrate crystal. This was an improvement on the state of the art. The seed beam at 873 nm that was created had a high quality mode. The 873 nm beam was sent into a chirped pulse non-collinear Raman amplifier. The first of its kind ever, the CPRA yielded good conversion efficiency to mJ energies while maintaining a good beam quality. The CPRA beam was sent into a novel compressor. The novel design was found using ZEMAX ray tracing program. Efficient compression was achieved, previously ps extent pulses were possible. One hundred fs high energy wavelength shifted pulses are now possible which are likely of high contrast. First Stokes (873 nm) ultrashort pulses have been produced at $>$ 10 GW level (2 mJ, 100 fs) for the first time ever. An anti-Stokes, higher frequency, Raman cascade of chirped laser pulses was produced for the first time. These colors are compressible following ZEMAX ray trace of their phase. Hence, a single cycle high energy system is demonstrated to be possible. High energy two color experiments are soon to be in progress using the CPRA.

Chapter 3

Construction of a Target for Two Color Experiments in Plasma and Future Work

3.1 Introduction

In this chapter, the construction of a target for two color experiments is outlined. Necessary properties of the target including a clean gas-vacuum interface are discussed. Construction, testing, and diagnostics of the laser produced plasma from the target are given. Future experiments including RS-LWFA using a two color high intensity source incident on a gas jet are then discussed and diagnostics of electrons produced from the interaction are given.

3.2 Gas Target for High Intensity Experiments

A gas target is needed for experiments in plasma. Laser ionization creates the plasma from the gas. A clean gas-vacuum interface is needed because ionization

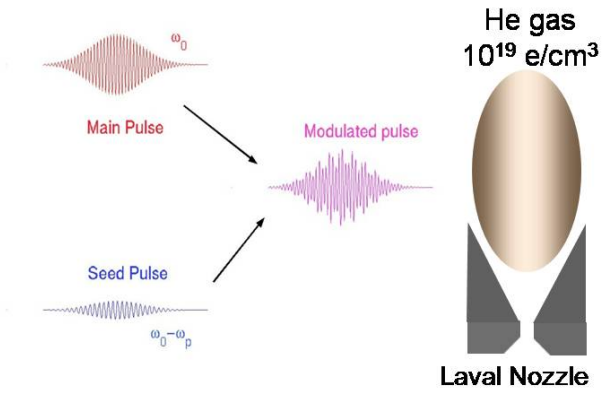

Figure 3.1: Schematic showing constriction in Laval nozzle allowing supersonic flow and incidence of two color laser.

induced defocusing and spectral shifts will distort the laser otherwise. A General Valve model 99 high pressure valve was used to produce a supersonic flow through various Laval valves. Interferometry was done to characterize the ionized gas region. An electron detection system suitable for use with very short time duration electron bunches was tested.

A Bergoz ICT was set up after the gas jet and the defocusing beam post target was blocked. Background electrons of low energy were detected synchronous with the arrival of the laser on target.

3.3 Diagnostics for Measuring Scattering from Plasma

A Bergoz Integrating Current Transformer (ICT) was used to detect background electrons when subjected to the pump. The ICT is basically a wire loop that is properly calibrated to measure charge that passes through it. Only background

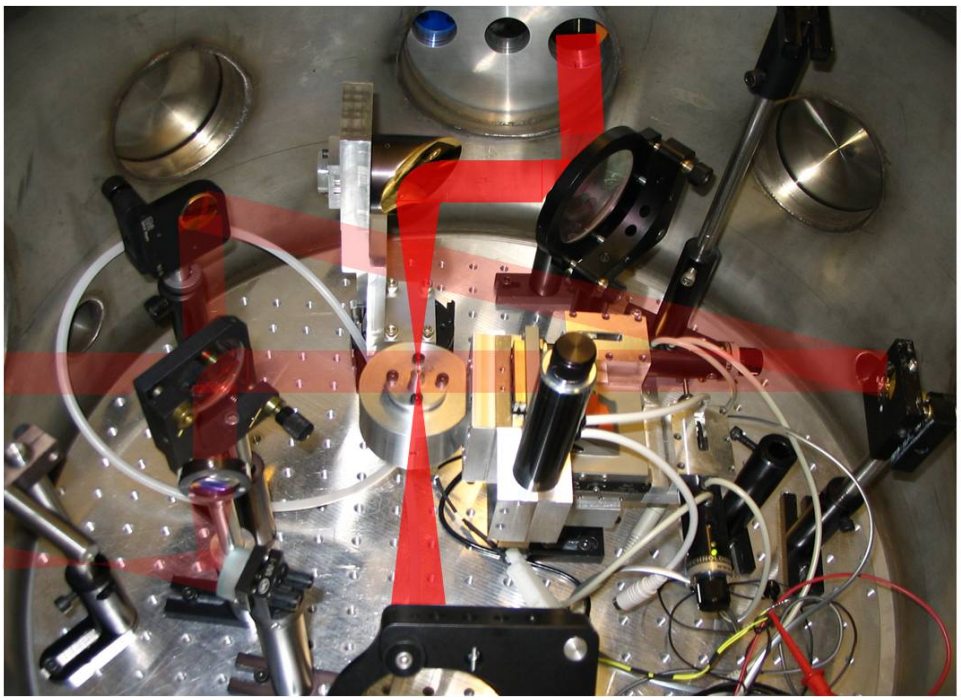

Figure 3.2: Experimental setup in vacuum chamber for two color experiments. Gas nozzle mounted on Zaber motor stage is in center. Nozzle could be externally moved through controls outside of chamber. The nozzle was positioned to have the laser enter the edge of the gas flow with minimal distortion.

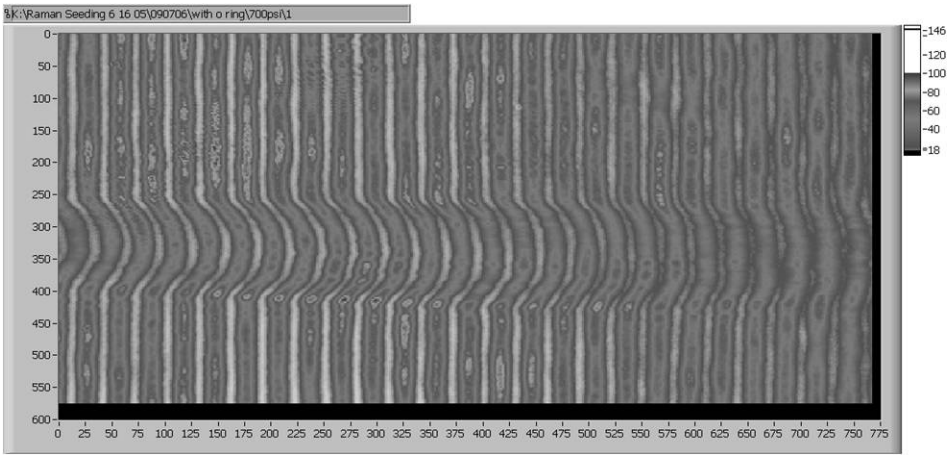

Figure 3.3: 700 PSI backing pressure ionized plasma interferogram. The defocusing of the laser is clearly visible.

electrons from the ionization process and the laser scattering off other objects was observed. A characteristic signal from the Bergoz ICT, recorded with a digital oscilloscope, is given here. The area under the curve is proportional to charge.

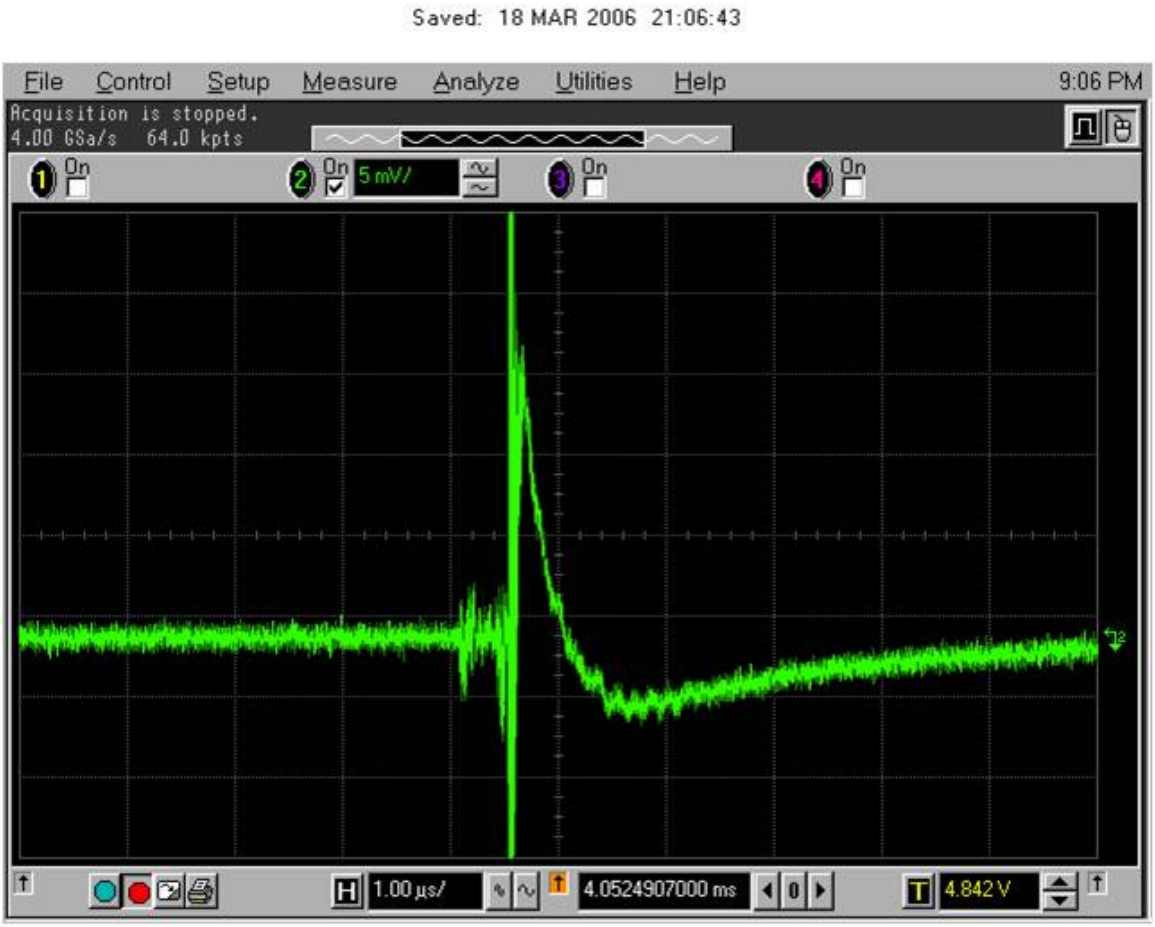

Figure 3.4: Bergoz ICT waveform from laser produced plasma. Low energy electrons are observed.

Many runs under many various conditions were undertaken with and without an aluminum foil in place to screen out low energy electrons. The laser pulse duration was attempted to be optimized in situ and the regenerative amplifier timing was

also attempted to be optimized in situ. Relativistic electrons were not observed, but a good diagnostic for their presence was tested and put in place.

3.4 Future Work

In the new, upgraded Tri-Color laser laboratory, one area of future work with the Chirped Pulse Raman Amplifier (CPRA) is the addition of an amplifier stage after the CPRA. The amplifier is a Ti:Sapph based six pass bowtie amplifier, see figure 3.4. The goal is amplify up to over 200 mJ energy. The compressed 873 nm Stokes beam would have a greater than 5 TW power. This is enough that at full energy it could produce its own wakefield. In addition, beatnote amplification experiments requiring TW power would be possible. An exciting future application of the RS-LWFA is a

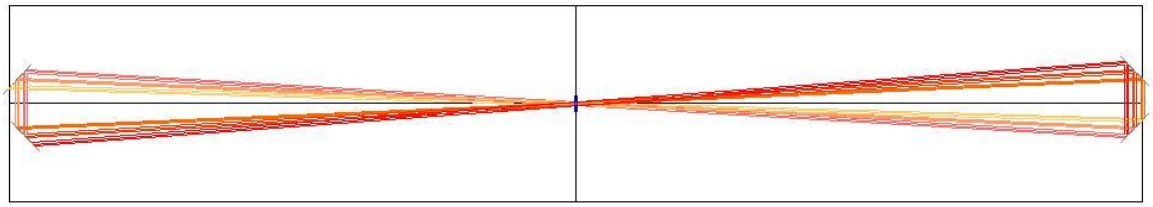

Figure 3.5: Autocad drawing showing the six pass Ti:Sapph amplifier for the CPRA beam. The crystal is at center. Figure from J.C. Sanders.

guided, channelled RS-LWFA building on the work of Gaul and Zgadzaj[2]. Figure 3.6 is a schematic showing the effect of the channel. Actual data of the exit mode with and without guiding is also shown. The long path length for the interaction given will help give a stable and controlled interaction[15]. The laser pulse can have a power below the critical power for self-focusing in plasma which makes it less vulnerable to transverse effects which can destabilize the interaction[3]. Fomyts'kyi showed that as little as 20 mJ pump with a 1 mJ seed can produce roughly nC amounts of relativistic charge[3]. In addition, the Raman Seed may be able to

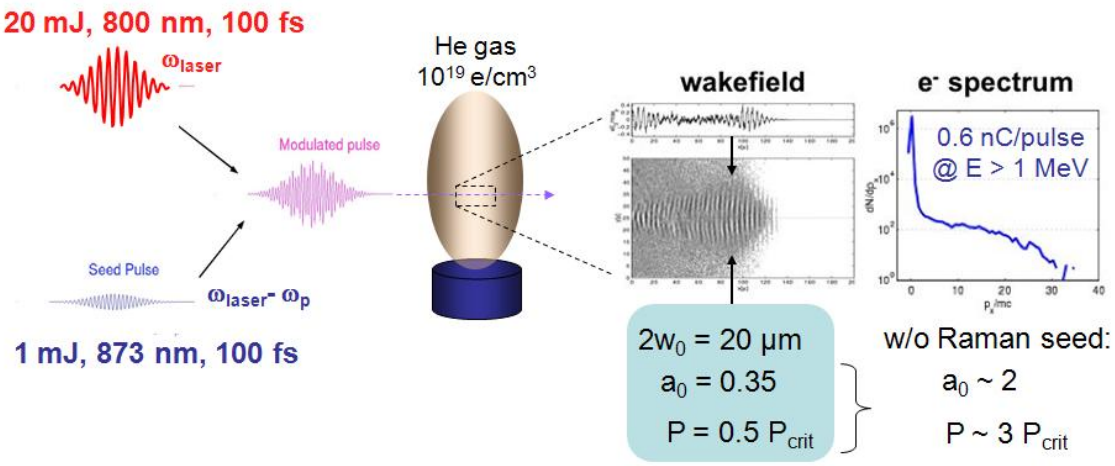

Figure 3.6: Schematic showing modulation of driver pulse, gas jet, and wakefield produced. Note that for the same electron spectrum in an unseeded case, the threshold power needed is much higher.

control the injection time in a staged channelled RS-LWFA. Controlling the timing allows control over the phase of the beam of electrons relative to the accelerating portion of the plasma wave[3]. By having stages of channelled RS-LWFA, with the gain in each stage at maximum due to the dephasing length, the dephasing length can be overcome and very high energies may be reached. The two color high energy CPRA makes such coherent control of the wake possible.

3.5 Conclusion

A gas jet using a high speed gas valve and a Laval nozzle was constructed to yield a supersonic gas flow. A relatively flat region of gas was generated with good gas vacuum interface necessary for high intensity experiments. The gas profile was probed using interferometric measurements of the laser produced plasma and the focusing and defocusing of the laser was observed. A diagnostic for relativistic electron pro-

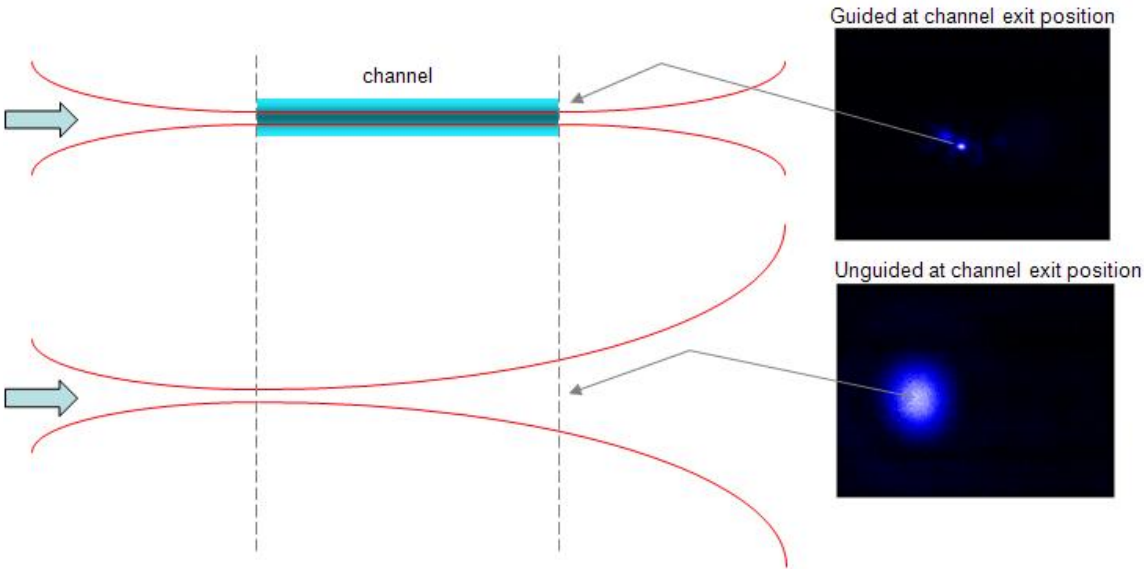

Figure 3.7: Schematic showing effect of channeling. Actual measured exit modes are shown. Note the focused beam waist is maintained throughout the channel. Data from Zgadzaj.

duction were put in place and tested. An Integrating Current Transformer (ICT) from Bergoz was used and detected background electrons from ionization. Looking for relativistic electrons gave a null result and the conclusion is that the pump laser power must be increased. The target and diagnostics give a good starting point for future experiments using the two color high intensity laser source. Such experiments are well characterized such as RS-LWFA and likely will be undertaken soon.

Appendix A

Parabolic mirror theory and alignment

Presented here is the theory behind Off Axis Parabolic Mirror (OAPM) alignment. OAPM alignment is defined by the normal to the paraboloid center as shown in figure A.1 below. An aligned, perfect parabola may undergo a pure translation and it will still be "aligned". The focal spot size will change by a factor of 2 in going from 0 to 90 degrees. For theoretical discussions of the off-axis parabolic mirror and its alignment, refer to the figure below which defines the relevant parameters implicitly.

The focal length of the parent paraboloid from which an off axis parabolic mirror (OAP) is patterned after is given by f. All rays incident with directions parallel to the y axis, the axis of the paraboloid, will come to a focus at the point drawn in the figure (0,f). For a ray incident at a distance x from the axis, it will traverse a distance f' in order to get to the focus. The effective focal length of this ray is f'. The half angle that it makes in reflecting off the parabola is $\beta/2$. As one can see

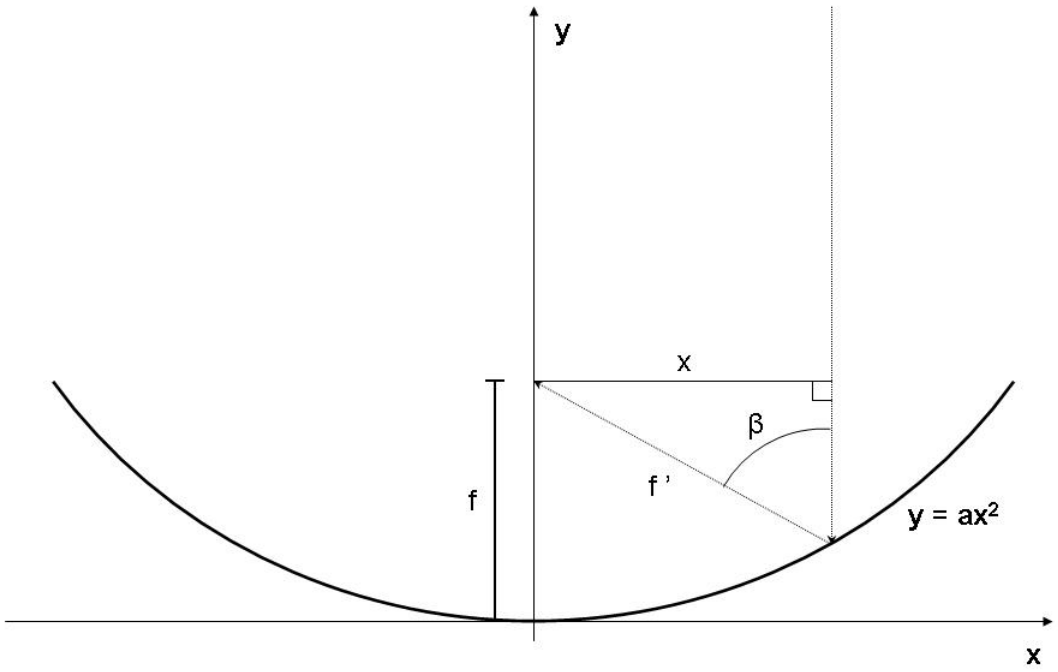

Figure A.1: Parabolic mirror is shown with light incident at a distance x from the axis. The vector defining the axis of the parabola lies along the axis y.

from the diagram, $f' = x/\sin\beta$. The tangent to the parabola at any point has a slope $2ax$. Now refer to the next figure, the triangle constructed with the tangent to the parabola has sides 2ax and 1. Consequently, $\tan(\beta/2) = 2ax$ and any such similar triangle constructed will give the same value for the tangent. Let us make the definition $f_o \equiv \frac{1}{4a}$. Now, solving for x yields $x = 2f_o \tan\beta/2$. Completing the derivation,

$$f' = \frac{x}{\sin\beta} = \frac{x}{\sin\left(2\tan^{-1}(2ax)\right)} \tag{A.1}$$

$$f' = \frac{x}{2\sin\left(\tan^{-1}(2ax)\right)\cos\left(\tan^{-1}(2ax)\right)} \tag{A.2}$$

$$f' = \frac{x}{2\frac{2ax}{\sqrt{1+4a^2x^2}}\frac{1}{\sqrt{1+4a^2x^2}}} \tag{A.3}$$

$$f' = \frac{x(1+4a^2x^2)}{4ax} \tag{A.4}$$

$$f' = \frac{1}{4a}(1+4a^2x^2) \tag{A.5}$$

$$f_o \equiv \frac{1}{4a} \tag{A.6}$$

$$f' = f_o(1+\frac{x^2}{(4f_o)^2}) \tag{A.7}$$

$$x = 2f_o\tan\beta/2 \tag{A.8}$$

$$f' = f_o(1+\tan^2\beta/2) \tag{A.9}$$

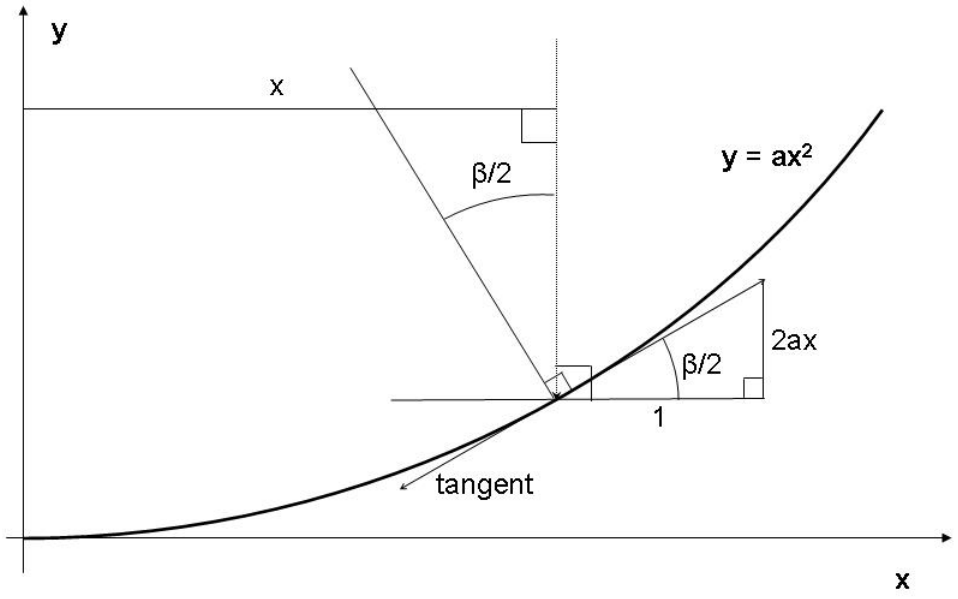

Figure A.2: OAPM showing tangent to the surface

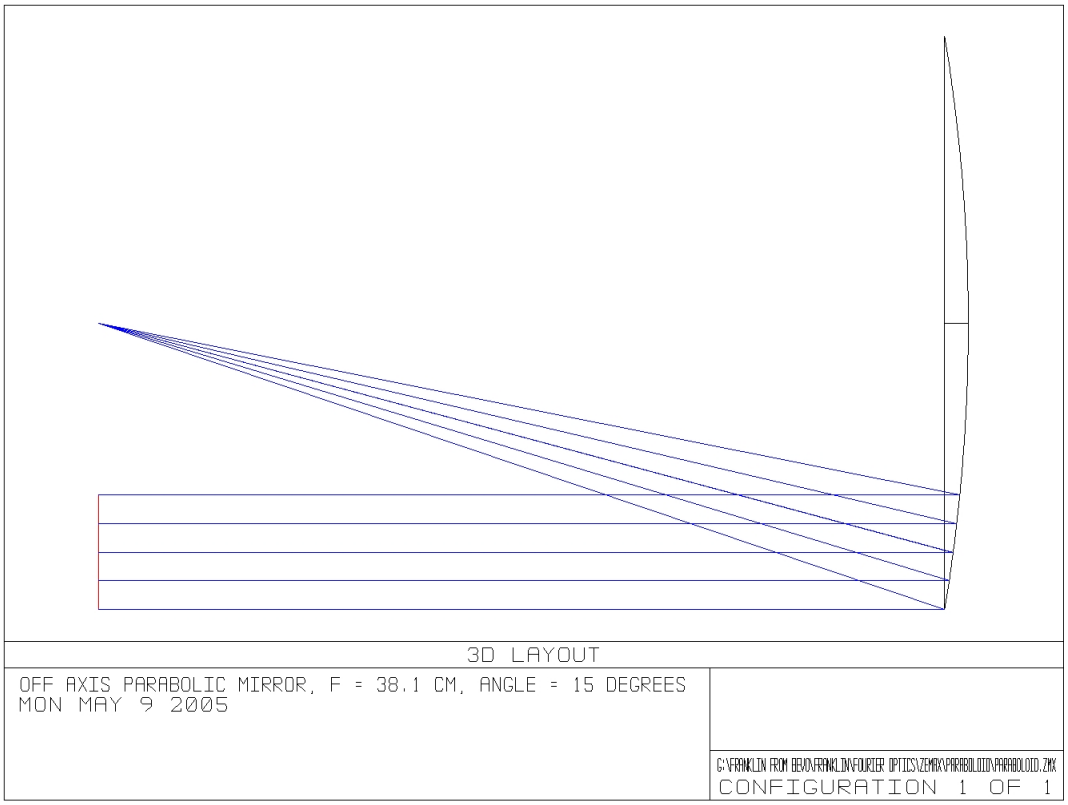

Figure A.3: ZEMAX raytrace diagram of a f = 38.1 cm parabola at 15 degrees off axis

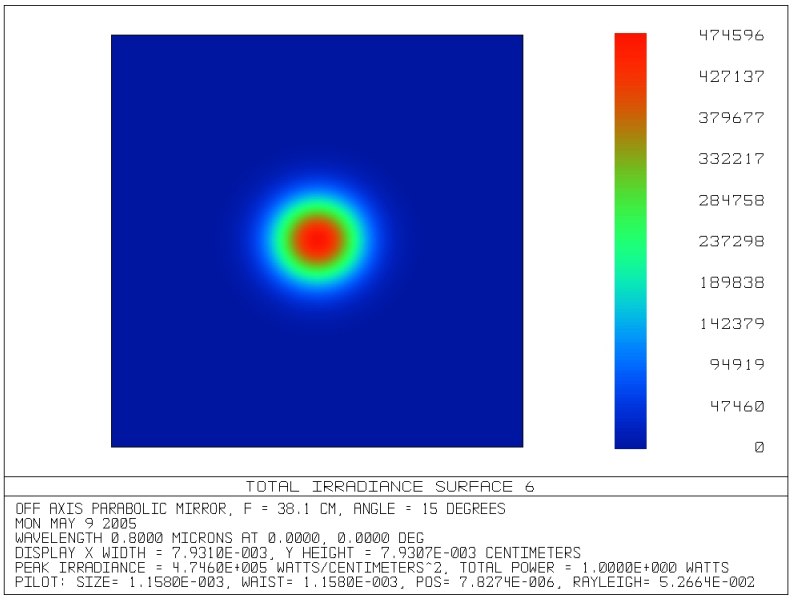

Figure A.4: ZEMAX diffraction calculation of the gaussian spot from the f = 38.1 cm parabola at 15 degrees off axis

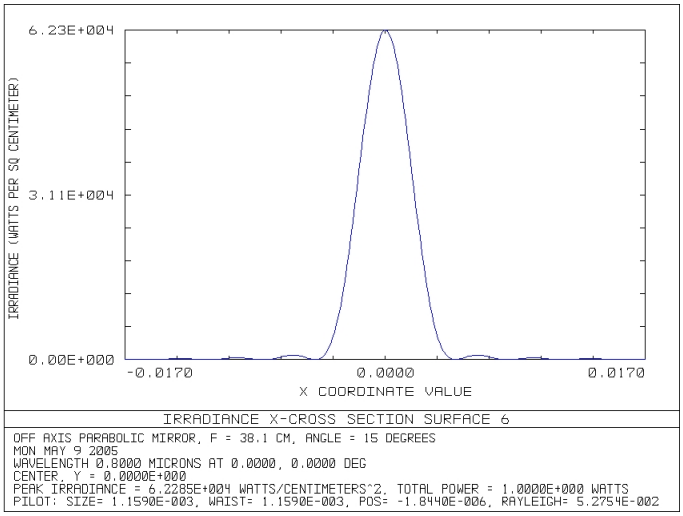

Figure A.5: ZEMAX diffraction calculation lineout of the focus from a beam apertured to 8.6 mm diameter (roughly a flattop) through a 38.1 cm OAPM at 15 degrees off axis

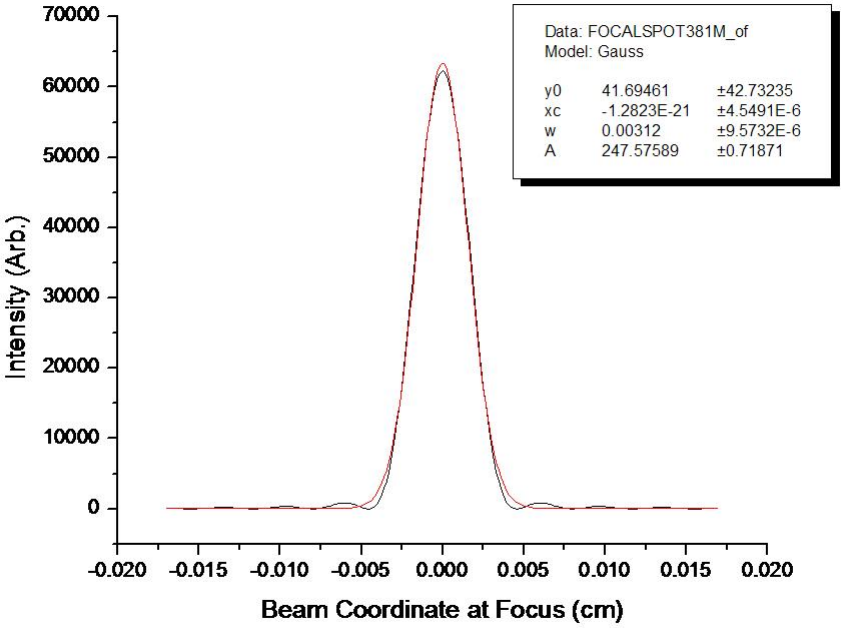

Figure A.6: ZEMAX diffraction calculation lineout of the focus from a beam apertured to 8.6 mm diameter (roughly a flattop) through a 38.1 cm OAPM at 15 degrees off axis exported to Labview and fit with a gaussian $w_o = 31$ μm

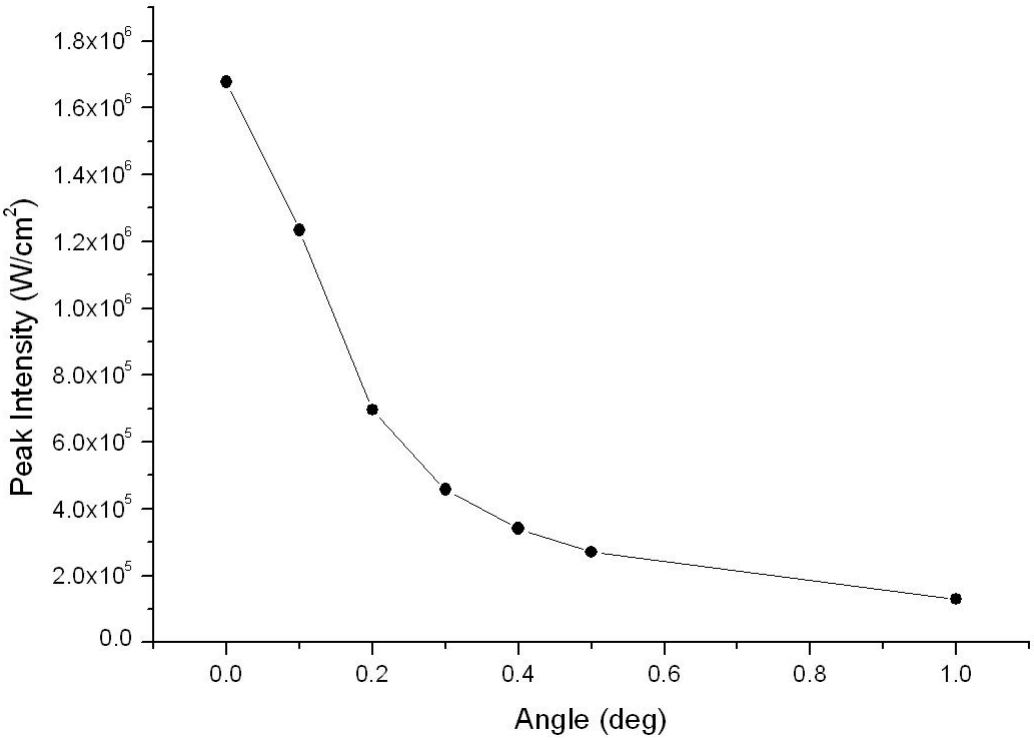

Figure A.7: ZEMAX diffraction calculation of the peak intensity at focus from a 38.1 cm OAPM at 15 degrees off axis, 800 nm light, vs a misalignment angle. Notice that a misalignment of 0.1 degrees yields a 25% drop in intensity. The input w_o = 1.6 cm.

A.1 Measurements of Off Axis Parabola Alignment

Real laser beams are aberrated. They can be fit by gaussians, but have deviations from gaussian beam propagation that can be significant. The focus of the laser beam allows one to look at the wavevector content of a laser beam. Aberrations show up in the focal plane. As Born and Wolf have shown in their book on the Principles of Optics[12], the primary aberrations have characteristic features in the focal plane. The actual focus of the pre-amplified laser beam is given below. It was measured with a CCD a large distance from the focus using a multi-element photographic lens in a configuration yielding high magnification. Small features on a resolution test target available from Newport calibrated the image. The unfocused beam had waists in the x and y directions of 8.24 mm and 8.8 mm, respectively. At focus, the laser focused to a spot of 14.6 μm and 14.1 μm, respectively.

For comparison to theory, the laser was aperatured to a diameter of 8.6 mm and the focus of the aperatured beam was measured. Note that significant energy is lost by aperaturing the beam tightly as was done. By reducing the f number, through use of the aperture, the aberrations at focus are reduced and comparison with theory is possible. At focus, the aperatured laser focused to a spot of 32.6 μm and 32.5 μm, respectively. Note that the calibration of the aperatured beam is different and was it was taken on a different data run than the unaperatured beam.

The agreement with theory of the focus of the apertured beam, both in numerical waist and qualitative features, gives much confidence in the results of the ZEMAX diffraction calculations. ZEMAX provides a powerful tool for both raytracing and actual diffraction calculations of the beam evolution which allows

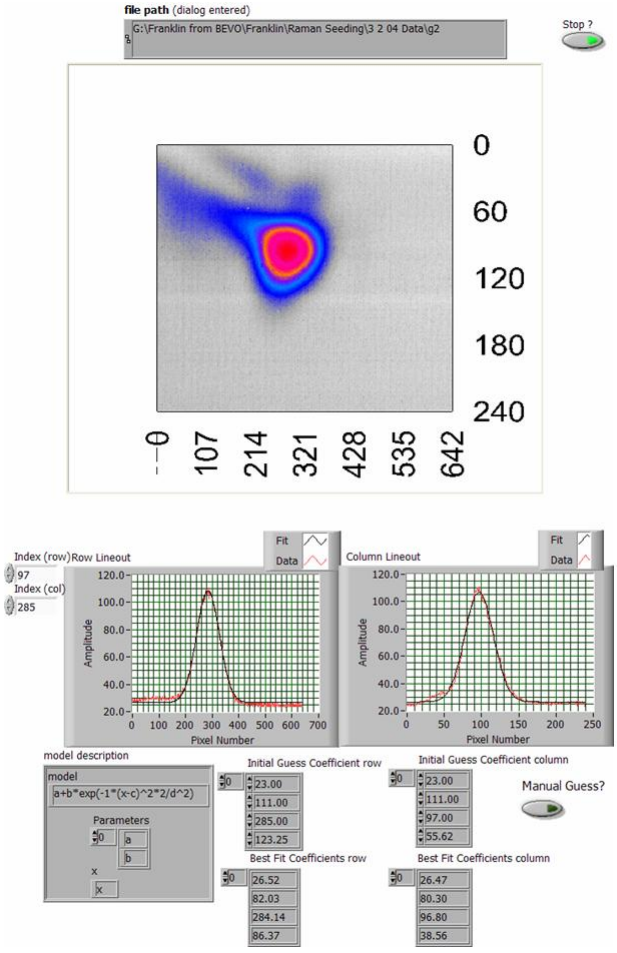

Figure A.8: Focus from a f = 38.1 cm OAPM at 15 degrees off axis.

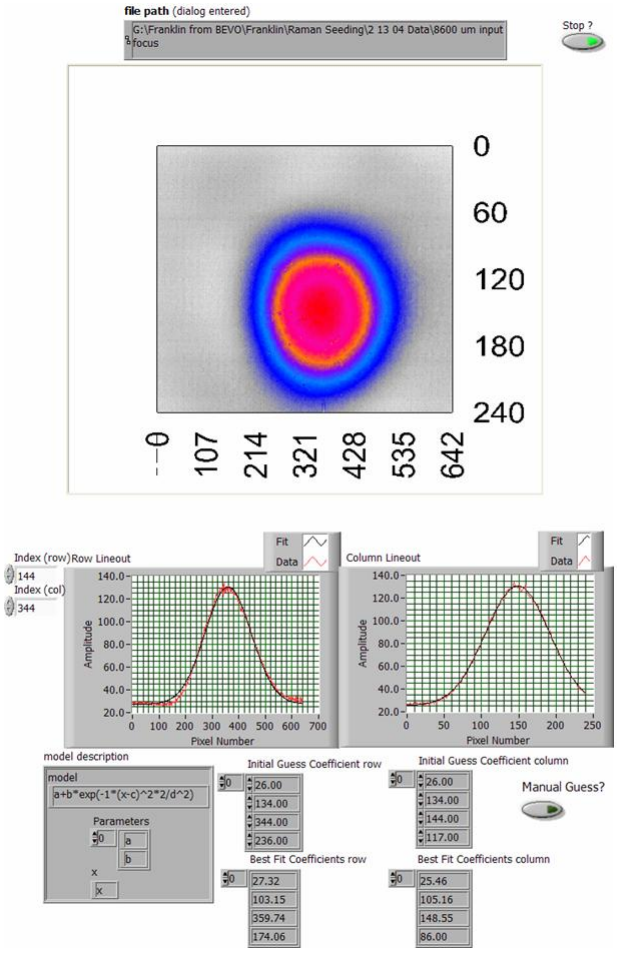

Figure A.9: Apertured beam focus from 38.1 cm OAPM at 15 degrees off axis showing good agreement with theory.

design of experimental apparatus and, sometimes more importantly, alignment of those systems.

Appendix B

Low n_2 Windows: Bandgap dependence

In a compressor that is open to the air, the transfer of the beam to a target chamber that is evacuated requires a window of some material with a n2 to enter the vacuum. High energy systems need a low n_2 material as they will often operate at a level such that spatial beam quality will degrade and the focused intensity will decrease due to a spatially varying $n_2 I(r)$ phase. In addition the temporal characteristics and spectrum will be affected in a related fashion when dispersion in the material is taken into consideration. After searching the literature, I found that there is a strong dependence on the bandgap of a window material and the n_2 of the material. The closer a material's cutoff wavelength to the wavelength of the beam, the larger the n_2 with a very strong dependence of 3.3 power, roughly. If you halve the bandgap energy, then you increase n2 by about an order of magnitude. The most attractive materials for windows for an 800 nm beam are MgF_2 and LiF. CVI and other companies make relatively inexpensive MgF_2 windows and have AR coatings at 800 nm making MgF_2 the natural candidate for high energy windows for Ti:Sapph laser systems where n_2 is a concern. In addition, it should be noted that BK7 is

significantly worse than UV grade Fused Silica.

MgF_2 was selected as the material of choice for the main 4 TW 800 nm beam. Square MgF_2 or LiF windows are not offered from any large vendor at the time of implementation. Newport and CVI did not carry them. The cost of optically flat, large blank uncoated MgF_2 windows was very high. Corning Optovac wanted a minimum order of $5000 for an order of windows. However, CVI had an available window in a 2" diameter with a standard AR coating at 800 nm. The CVI bid for W2-P2-2019-MF-633-1064-0 was only $485, MgF_2 two surface AR coated window 633 nm - 1064 nm. This window was implemented in 2002 and it worked very well at low cost. Noticeable filamentation or self-phase modulation was not observed. Other members of the group made attempts at noticing negative effects of the window on the beam and concluded it was good. Replacing it with a standard glass window, showed broadband self-phase modulation observable by eye.

Appendix C

Derivation of Time-Bandwidth product for Gaussian Lasers Pulses

Here is a quick derivation of the time bandwidth product for laser pulses. Start with the Heisenberg Uncertainty principle.

$\Delta E \Delta t \geq \hbar/2$

$E = \hbar\omega$

$\Delta\omega = \sigma_\omega/\sqrt{2}$

$\Delta t = \sigma_t/\sqrt{2}$

This follows from the definition of Gaussian laser pulses in time and hence frequency.

Hence, $\sigma_t \sigma_\omega = 1$

For a Gaussian, $\exp(-t^2/2\sigma_t^2)$, $t_{fwhm} = 2\sqrt{\ln 2}\sigma_t$.

Subsituting, $t_{fwhm}\omega_{fwhm} = 4\ln 2$ which leads to $t_{fwhm}\lambda_{fwhm} = 2\ln 2\lambda^2/\pi c$.

For 800 nm light, $t_{fwhm}\lambda_{fwhm} = 941.38nmfs$.

$30nm \Leftrightarrow 31.4fs$

Appendix D

Residual Fourth Order Dispersion of the Stretcher Dependent on Image Inverter Location

The Barty-Lemoff stretcher design is very sensitive to alignment due to its design[11]. Astigmatism is introduced when the beam goes off the cylindrical mirrors (see figure D.1). A ZEMAX raytrace was conducted of the stretcher. Using macros written in the program language native to ZEMAX, the phase was traced through the stretcher. The beam was then traced through the rest of the CPA system accounting for the dispersion of all the material in the laser chain. Finally, the compressor angle and separation were chosen by optimizing the output compression of the laser pulse. Using such a routine, parameters of the laser system can be adjusted and the optimized (best case) output laser pulse can be compared. A graph is given below in figure D.1 that shows how the fourth order residual dispersion of the system can be zeroed

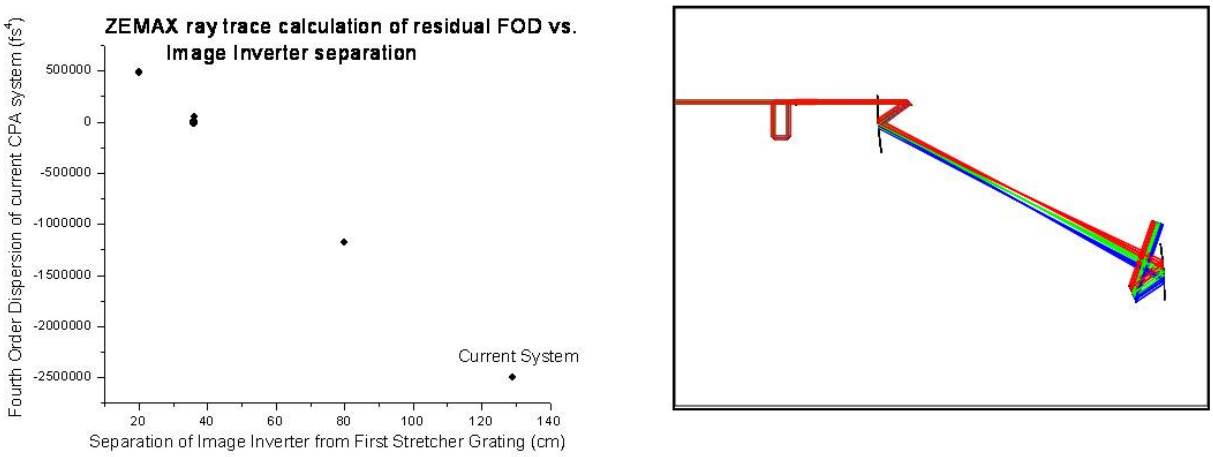

Figure D.1: On left, graph of ZEMAX calculated residual FOD of the compressed laser pulses vs the position of the Image Inverter. On the Right, the ZEMAX raytrace diagram of the stretcher, image inverter is at left.

by moving the image inverter of the Lemoff stretcher. The image inverter flips the beam around, inverting the image and sending it back through for one more round trip pass through the stretcher. Different colors are diverging slightly after the first pass which explains how the image inverter can affect the residual FOD. The actual image inverter was moved, but bandwidth issues and other compression issues prevented observation of whether the FOD was changed. Doing a Frequency Resolved Optical Gating (FROG) before and after the movement of the image inverter would be an interesting experiment. Overall, in the future, optimization routines as was written provide a valuable tool for creating very well compressed laser pulses. All parameters can be explored. Even those that at first sight, do not appear to be relevant to the phase of the output pulse.

Appendix E

CPA laser at 800 nm

In order that CPRA could be achieved, a suitable 800 nm laser must be present. The beam quality, energy, polarization, pre-pulse contrast ratio, and stability need to be of good quality. The Titanium doped Sapphire laser yielded pulses to the interaction chamber of 300 mJ energy and 80 fs compressed pulse duration at 10 Hz repetition rate. The CPA laser chain consisted of a Ti:Sapph oscillator at 800 nm with a bandwidth of between 20-30 nm depending on how it was tuned. Great effort was needed to get it operating at specification for experiments.

E.1 Oscillator

The oscillator, see figure E.1, was home-built and required tuning before the start of operation of the CPA system every day. The oscillator was pumped by a 3.5 W Millenia V from Spectra Physics 532 nm CW laser. The Millenia V was the pump laser incident on a 10 mm long Brewster-cut Ti:Sapphire crystal. Two intra-cavity prisms are used to compensate for the dispersion of the crystal. The output coupler (OC) that was used transmitted about 12% of the energy [10]. One problem encountered was that thermal variations during the day and night could affect the

laser cavity and cause it to fall out of mode-locked operation. The laser would no longer produce short pulses, but would be in continuous wave mode due to these thermal variations or sometimes large vibrations or shocks to the optical table. The work of Bonggu Shim and others in our group on the system stabilized the oscillator greatly [10]. The oscillator put out 9 nJ pulses with a 30 nm bandwidth at a repetition rate of 76 MHz. The oscillator was synched with a high energy 1064 nm YAG system used to produce plasma waveguide channels. The YAG system completed the tri-color UT laser system, 800 nm, 873 nm, and 1064 nm (though a fourth color, 800 nm second harmonic at 400 nm, was also available).

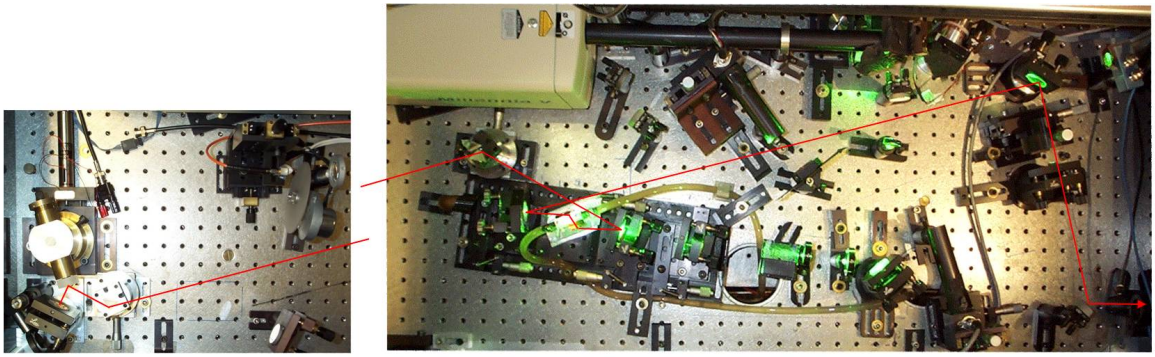

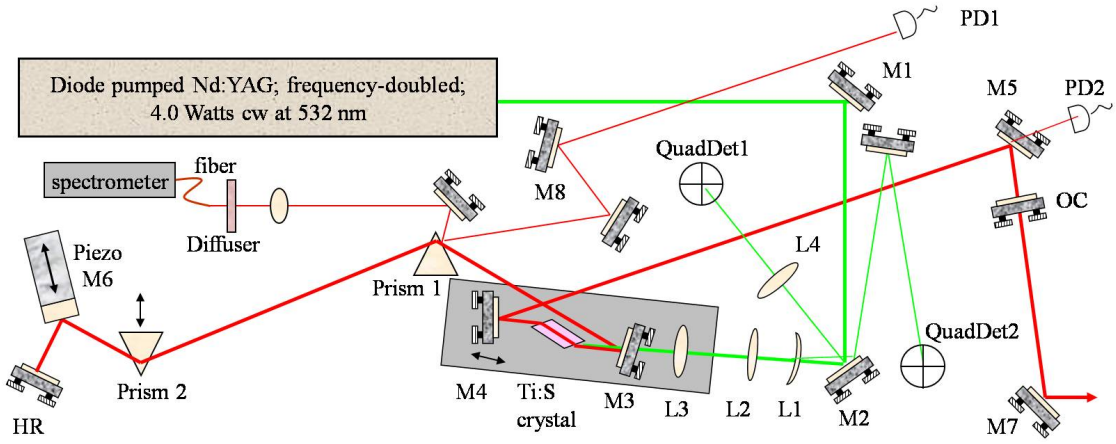

Figure E.1: 800 nm Oscillator.

E.2 Subsystems of the Ti:Sapphire CPA system

E.2.1 Stretcher

Following the oscillator, is the stretcher which is of the Lemoff and Barty design [11]. The stretcher design and alignment greatly affects the temporal and transverse properties of the laser pulse. The two properties are linked together because different colors undergo different paths through the stretcher, as ray traces show, and so aberrations in the beam in space become changes in phase in the compressed beam

in time. The final output bandwidth of the laser system was around 20 nm. 20 nm was stretched to about 200 ps in the stretcher. Two antiparallel gratings (1200 lines/mm) with a telescope of two cylindrical mirrors coated in gold (curvature 1 m) were used, see figure 3.2. The angle of incidence of the gratings was adjusted during the system's lifetime, but was typically 61.9 %. An image inverter is used to reflect the beam back through the system. See Appendix D for additional discussion of the image inverter. After the stretcher, the beam is sent to the regenerative amplifier.

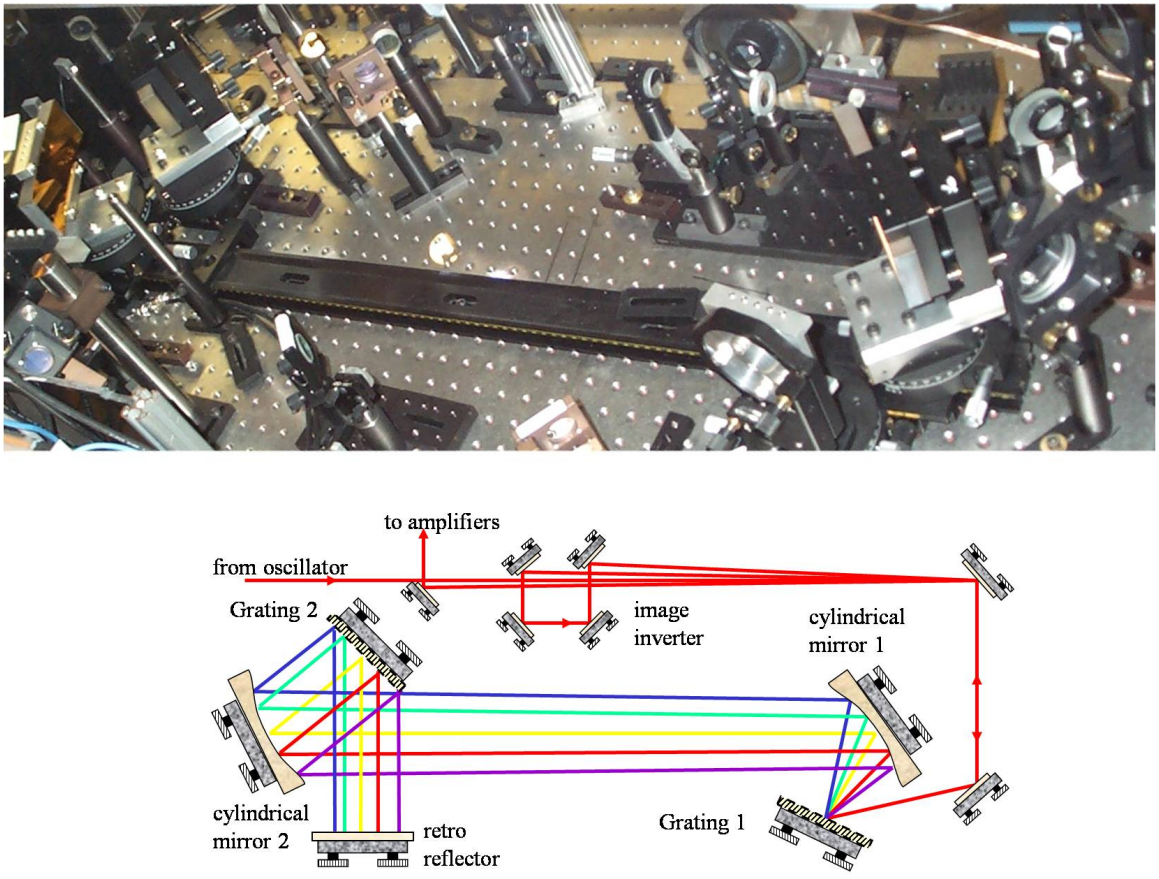

Figure E.2: Stretcher

E.2.2 Regenerative Amplifier

The regenerative amplifier works by trapping a pulse in a cavity through use of the Pockels effect. High voltage is used to change the polarization of the incoming pulse passing through a Pockels cell. The regenerative amplifier picks one pulse off the MHz pulse train and cuts the repetition rate to 10 Hz through control of the Pockels cell. The pulse then is transmitted through the Thin Film Polarizer (TFP2) and is trapped in the cavity containing the Ti:Sapph crystal which produces gain. The pulse undergoes about 28-30 passes in the regenerative amplifier depending on oscillator performance and regen alignment. The total gain experienced is about 10^6 yielding an output energy of 1 mJ. As the regen is a cavity, coupled with the high, saturated gain, the regen produces a very good output mode. The Pockels cell is fired again and the pulse exists the regenerative amplifier and heads over to the pre-amplifier.

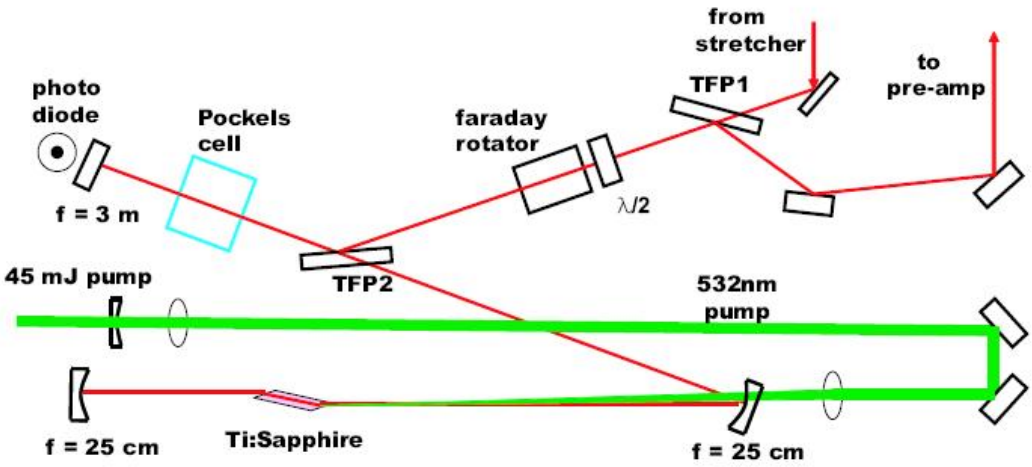

Figure E.3: Regenerative Amplifier courtesy of B. Shim

E.2.3 Pre-Amplifier and Power Amplifier

The pre-amplifier is a 4 pass bow tie multi-pass Ti:Sapph amplifier that provides a gain of ~ 200. The pre-amp is pumped by 600 mJ of 532 nm pulsed light from Q-switched lasers. Some of the light is residual light, 100 mJ, from the regen pump laser, a Surelite from Continuum. The bulk of the light, 500 mJ, comes from a Spectra-Physics GCR4. A relatively large, 1 cm long Ti:Sapph crystal is the gain medium. It has a custom made cooling jacket which water cools the crystal to prevent thermal damage over time. 30 mJ is split off here with a removable beam splitter and sent to the CPRA apparatus for shifting to 873 nm light. The output energy of the whole system is not greatly affected as the power amplifier is heavily saturated. The output is sent through a spatial filter to clean up the mode before the final amplification stage where damage is of most concern. The pre-amp and power-amp both suffered from damage and stability issues. The optics and crystal were both at constant risk of damage from hot spots in the beam. A spatial filter was installed between the two stages to help filter the 800 nm beam. Constant monitoring of the beam was necessary. The mode of the pump laser of the GCR used to pump the pre-amplifier Ti:Sapph crystal had an asymmetric shape after work by a contractor was done to upgrade the power and realign the cavity. The compensator plate was removed and the mode took on a star like appearance. Some of this mode was transferred to the 800 nm CPA beam. However, the spatial filter did help and the three different beam lines as well as the use of some of the Surelite energy helped in creating a more homogenous pumped volume in the crystal. The mode of the GCR pump laser had to be constantly monitored on a weekly, even daily basis as a misalignment would lead to a mode that could damage the valuable Ti:Sapph crystal.

Spatial filters were set up in some of the lines of the pump lasers to yield a smoother, more uniform beam profile at the crystal. A circular filter placed at focus

will yield a smoother beam at output because by the fourier optics of the design, the output beam will be the convolution of the transform of the circle or a sinc function with the input beam which will smooth it. The output of the spatial filter is sent to the power amplifier.

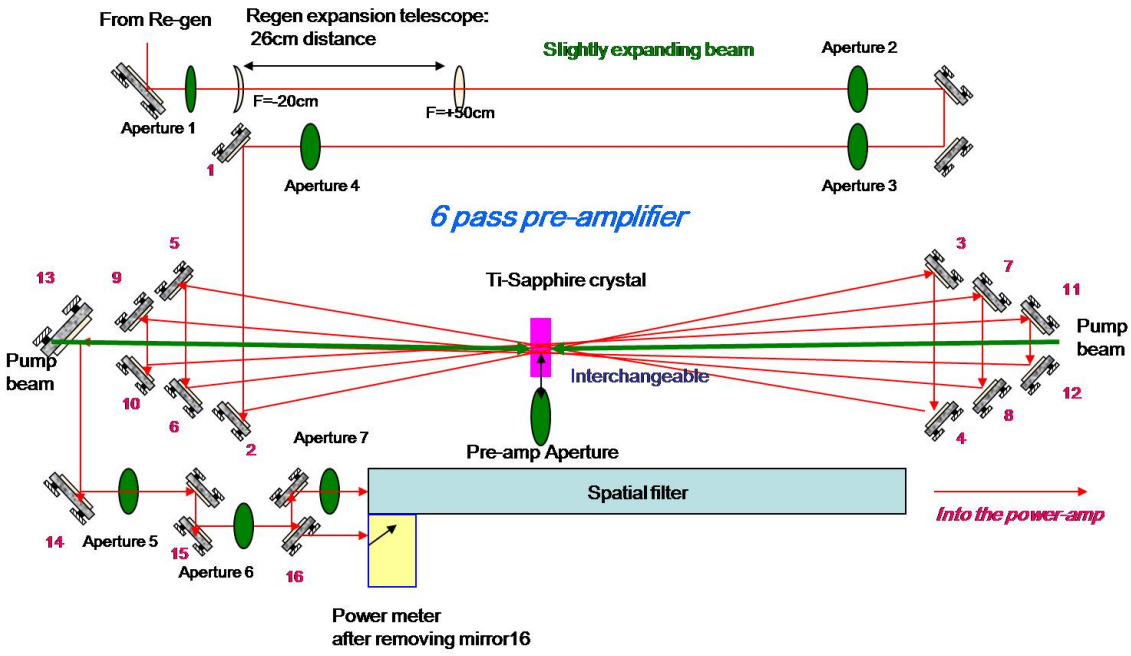

Figure E.4: Pre-amplifier

The power amplifier provides a gain of 3.5 in four passes. The gain is heavily saturated here. The power amplifier is pumped by a 1.1 J Pro350 from Spectra-Physics which is a Nd:YAG laser. The power amplifier is the final stage of ampli-

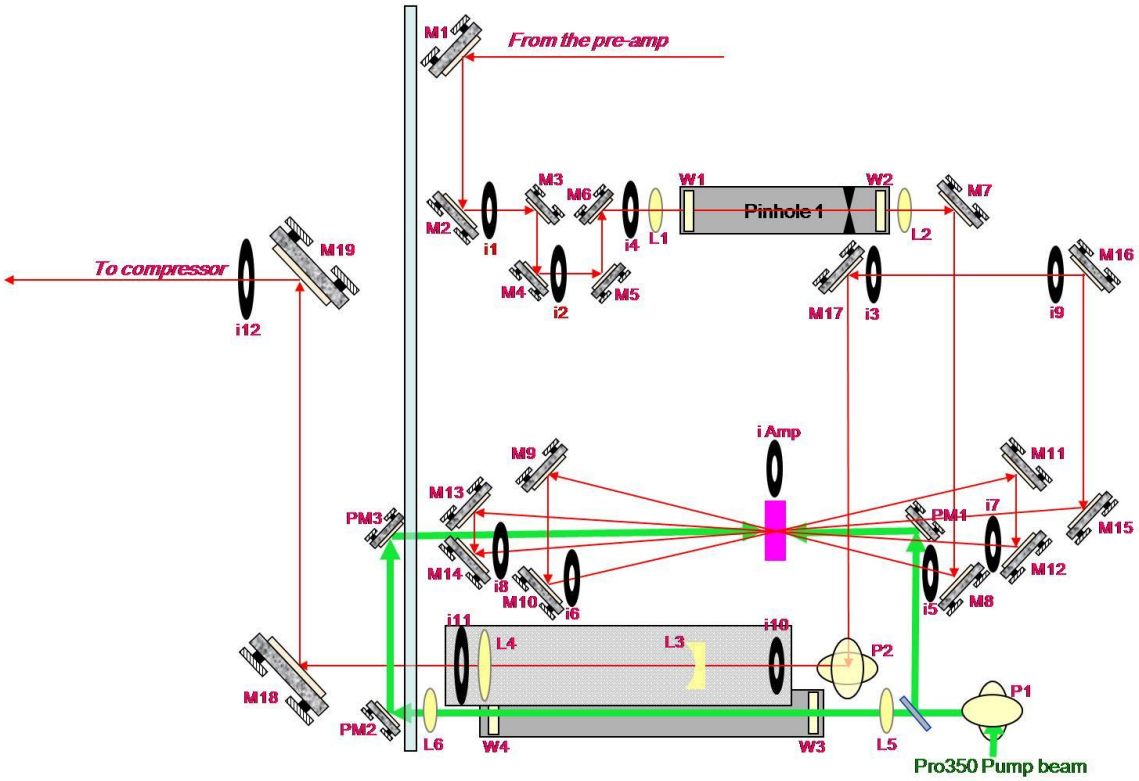

Figure E.5: Power Amplifier Alignment

fication before the compressor and the target chamber. The energy is the highest here so the beam is the most difficult to work with and damage is constantly and issue. The optics need to be often inspected with a fiber light for signs of initial signs of damage. The mount for the power amplifier Ti:Sapph crystal has a special annular ND filter to absorb the edge of the pump and Ti:Sapph beams and prevent ablation of material from the cooling jacket. Ablation from the metal cooling jacket can deposit no the crystal. To analyze the performance of the pre and power amplifiers, models were constructed to analyze the gain and thermal lensing[10]. Good agreement was found.

E.2.4 Compressor

The compressor uses two gold coated gratings of 1200 line/mm line density to produce negative dispersion and compress the beam. The incidence angle is 69 degrees. The output pulses from the compressor had an energy up to 300 mJ with a typical pulse length of 80 fs.

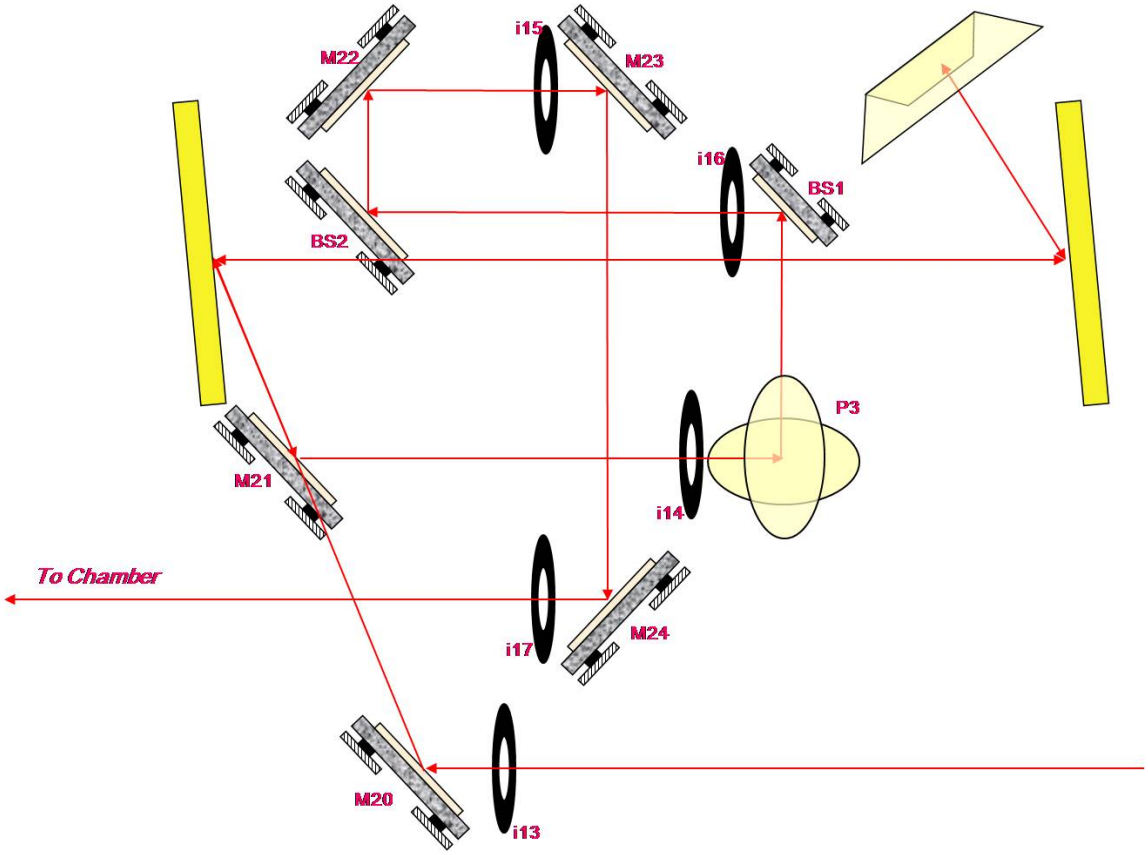

Figure E.6: Compressor

Characterization of pump laser and Ti:sapph beams by CCD and energy measurements. A precise mapping of the fluence of the beam is a common feature of high energy laser work. The precise imaging of the beam to the scientific, linear camera must be done properly. Several formulas were derived from basic optics formulas to yield distances at which lenses should be placed. For a magnification M, object distance o = (M+1)/M f and for image distance i = (M+1)f. A calibration test target designed by the Air Force and sold commercially by many vendors was used in the object plane to give a length scale on the image plane placed at the CCD of the camera.

An obstacle to progress with the experiment was temperature variations during the day. As the temperature changed during the day/night cycle, the optical table and the parts on it would undergo an expansion or contraction depending on the local change in temperature. This would change the alignment of the beam at the chamber and would affect the energy. The alignment through the amplifier stages would determine the amplification as passing very close through the gain region was necessary. A temperature map of the lab was constructed using small temperature sensors placed inside the optical boxes. Optical boxes were used to enclose the area to reduce air currents and to prevent dust from falling on optics.

Bibliography

[1] T. Tajima and J. Dawson, "Laser Electron Accelerator," Phys. Rev. Lett. **43**, 267-270 (1979).

[2] R. Zgadzaj, E. Gaul, N. H. Matlis, G. Shvets and M. C. Downer, "Femtosecond pump-probe study of preformed plasma channels," J. Opt. Soc. Am. B **21**, 1559-1567 (2004).

[3] M. Fomytskyi, C. Chiu, M. C. Downer, F. Grigsby, "Controlled plasma wave generation and particle acceleration through seeding of the forward Raman scattering instability," Phys. Plasmas **12**, 023103 (2005).

[4] N. Zhavoronkov, F. Noack, V. Petrov, V. P. Kalosha, and J. Herrmann, "Chirped-pulse stimulated Raman scattering in barium nitrate with subsequent recompression," Opt. Lett. **26**, 47-49 (2001).

[5] S. Kalmykov and G. Shvets, "Compression of laser radiation in plasmas using electromagnetic cascading" Phys. Rev. Lett. **94**, 235001 (2005).

[6] F. Grigsby, P. Dong, and M. Downer, "Chirped-pulse Raman amplification for two-color, high-intensity laser experiments" J. Opt. Soc. Am. B. **25**, 346 (2008).

[7] J. T. Murray, W. L. Austin and R. C. Powell, "Intracavity Raman conversion and Raman beam cleanup," Opt. Mat. **11**, 353-371 (1999).

[8] A. I. Vodchits, V. P. Kozich, V. A. Orlovich, and P. A. Apanasevich "Z-Scan studies of KYW, KYbW, KGW, and $Ba(NO_3)_2$ crystals" Opt. Comm. **263**, 304-308 (2006).

[9] J. G. Wessel, K. S. Repasky, and J. L. Carlsten "Competition between spontaneous scattering and stimulated scattering in an injection-seeded Raman amplifier" Phys. Rev. A **53**, 1854-1861 (1996).

[10] B. Shim, *Time-Resolved Study of Third Harmonic Generation from Anisotropically Expanding Clusters, PhD. Thesis*, (University of Texas at Austin, 2006).

[11] B. E. Lemoff and C. P. J. Barty, Opt. Lett. **18**, 1651 (1993).

[12] M. Born and E. Wolf, *Principles of Optics, 7th Edition*, (Cambridge University Press, 2002).

[13] J. Squier, C. P. J. Barty, F. Salin, C. Le Blanc, and S. Kane, "Use of mismatched grating pairs in chirped-pulse amplification systems," App. Optics **37**, 9, 1638 (1998).

[14] A. V. Sokolov and S. E. Harris, "Subfemtosecond pulse generation by molecular modulation," Phys. Rev. A**55**, R4019 (1997).

[15] C.G.R Geddes et al., "High-quality electron beams from a laser wakefield accelerator using plasma-channel guiding," Nature **431**, 538-541 (2004).

Vita

Franklin Grigsby was born December 8, 1976 in Washington D.C, the son of Thomas Grigsby and Sarojini Grigsby. He received the Bachelor of Science degree in Physics from Harvey Mudd College in Claremont, CA. He applied to several graduate schools in Physics and was accepted at all of them, choosing to attend the University of Texas at Austin. He worked with electrically produced plasmas at Unison in Jacksonville, Florida before coming to graduate school in Austin.

Permanent Address: 1311 South Norwood Street
Arlington, Virginia 22204

This dissertation was typeset with LaTeX 2_ε[1] by the author.

[1] LaTeX 2_ε is an extension of LaTeX. LaTeX is a collection of macros for TeX. TeX is a trademark of the American Mathematical Society. The macros used in formatting this dissertation were written by Dinesh Das, Department of Computer Sciences, The University of Texas at Austin, and extended by Bert Kay and James A. Bednar.